

## Simulating aerosol-radiation-cloud feedbacks on meteorology and air quality over eastern China under severe haze conditions in winter

B. Zhang<sup>1,2</sup>, Y. Wang<sup>1,3,4</sup>, J. Hao<sup>2</sup>

<sup>1</sup> Ministry of Education Key Laboratory for Earth System Modeling, Center for Earth System Science, Institute for Global Change Studies, Tsinghua University, Beijing, 100084, China

<sup>2</sup>School of Environment, Tsinghua University, Beijing, 100084, China

<sup>3</sup>Department of Marine Sciences, Texas A&M University Galveston Campus, Galveston, TX, 77553, USA

<sup>4</sup>Department of Atmospheric Sciences, Texas A&M University, College Station, TX, 77843, USA.

Correspondence to: Yuxuan Wang

10 Phone: (+86)13701032461

11 Fax: (+86) 10-62781708

12 E-mail: yxw@mail.tsinghua.edu.cn

13

14 **ABSTRACT**

15 The aerosol-radiation-cloud feedbacks on meteorology and air quality over eastern China under severe winter haze  
16 conditions in January 2013 are simulated using the fully coupled on-line Weather Research and Forecasting/Chemistry  
17 (WRF-Chem) model. Three simulation scenarios including different aerosol configurations are undertaken to distinguish the  
18 aerosol radiative (direct and semi-direct) and indirect effects. Simulated spatial and temporal variations of PM<sub>2.5</sub> are  
19 generally consistent with surface observations, with a mean bias of  $-18.9 \mu\text{g}/\text{m}^3$  ( $-15.0\%$ ) averaged over 71 big cities in  
20 China. Comparisons between different scenarios reveal that aerosol radiative effects (direct effect and semi-direct effects)  
21 result in reductions of downward shortwave flux at the surface, 2 m temperature, 10 m wind speed and planetary boundary  
22 layer (PBL) height by up to  $84.0 \text{ W}/\text{m}^2$ ,  $3.2^\circ\text{C}$ ,  $0.8 \text{ m/s}$ , and  $268 \text{ m}$ , respectively. The simulated impact of the aerosol  
23 indirect effects is comparatively smaller. Through reducing the PBL height and stabilizing lower atmosphere, the aerosol  
24 effects lead to increases in surface concentrations of primary pollutants (CO and SO<sub>2</sub>). Surface O<sub>3</sub> mixing ratio is reduced  
25 by up to 6.9 ppb due to reduced incoming solar radiation and lower temperature, while the aerosol feedbacks on PM<sub>2.5</sub> mass  
26 concentrations show some spatial variations. Comparisons of model results with observations show that inclusion of aerosol  
27 feedbacks in the model significantly improves model performance in simulating meteorological variables and improves  
28 simulations of PM<sub>2.5</sub> temporal distributions over the North China Plain, the Yangtze River Delta, the Pearl River Delta, and  
29 Central China. Although the aerosol-radiation-cloud feedbacks on aerosol mass concentrations are subject to uncertainties,  
30 this work demonstrates the significance of aerosol-radiation-cloud feedbacks for real-time air quality forecasting under haze  
31 conditions.

32

33 **1. Introduction**

34 Atmospheric aerosols are known to play a key role in the earth climate system. They absorb and scatter incoming solar  
35 radiation, referred to as the direct effect (Hansen et al., 1997). They also alter cloud properties by serving as cloud  
36 condensation nuclei (CCN), which is known as the indirect effect (Albrecht, 1989; Twomey, 1977; Rosenfeld et al., 2008).  
37 Absorbing aerosols in and under the cloud may heat the atmosphere, leading to evaporation of clouds (semi-direct effect)  
38 (Charlson and Pilat, 1969). It is of increasing interest to understand and quantify the complex impacts of aerosols on  
39 meteorology and air quality. The coupled “on-line” meteorology-air quality strategy with aerosol feedbacks is essential for  
40 real-time air quality forecasting using 3-D models. Negligence of aerosol feedbacks may lead to poor performance of the  
41 next hour’s meteorology and air quality forecasting, especially for high aerosol loading regions (Grell and Baklanov, 2011;  
42 Zhang et al., 2012).

43 Models simulating the direct, indirect, and semi-direct effects of aerosols on meteorology and chemistry need to couple  
44 aerosols with physical and chemical processes. The chemistry version of Weather Research and Forecasting (WRF-Chem)  
45 model (Grell et al., 2005) is a state-of-the-art meso-scale “on-line” atmospheric model, in which the chemical processes and  
46 meteorology are simulated simultaneously. This design makes WRF-Chem capable of simulating aerosol feedbacks on  
47 various atmospheric processes. Several studies employing WRF-Chem reveal that aerosols reduce downward solar radiation  
48 reaching the ground, inhibit convection, reduce the PBL, hence make the lower atmosphere more stable (Fan et al., 2008;  
49 Forkel et al., 2012; Zhang et al., 2010). WRF-Chem results also indicate that aerosols can modify atmospheric circulation  
50 systems, resulting in changes in monsoon strength, precipitation distribution, and mid-latitude cyclones (Zhao et al., 2011;  
51 Zhao et al., 2012).

52 In January 2013, several severe and long-lasting haze episodes appeared in eastern China (Figure 1). Monthly mean  
53 mass concentrations of fine particulate matters ( $PM_{2.5}$ ) exceeded  $200 \mu g/m^3$  in some cities in North China Plain.  
54 Meteorological conditions and chemical components of  $PM_{2.5}$  during this month have been investigated by a number of  
55 studies in order to understand the chemical characteristics and formation mechanism of severe winter haze episodes (Bi et  
56 al., 2014; Che et al., 2014; Huang, K. et al., 2014; Sun et al., 2014; Wang, L. T. et al., 2014; Wang, Y. S. et al., 2014; Wang,  
57 Y. X. et al., 2014; Wang, Z. F. et al., 2014; Zhang, J. K. et al., 2014). Meanwhile, such high levels of PM concentrations are  
58 expected to exert impacts on meteorological conditions through the aerosol-radiation-cloud interactions. Few of current air  
59 quality forecasting systems for China include aerosol-meteorology interactions. The significance of this effect and the extent  
60 to which it feedbacks on air quality remains to be uncertain and needs to be quantified for better forecasting air quality in  
61 China in the future (Wang et al., 2013; Zhang, Y. et al., 2014; Wang, Z. F. et al., 2014).

62 In this work, the fully coupled “on-line” WRF-Chem model is employed to simulate the complex interactions between  
63 aerosols and meteorology and to characterize and quantify the influences of aerosol feedbacks on meteorology and air  
64 quality under severe winter haze conditions in January 2013 over eastern China. The aerosol direct, indirect and semi-direct  
65 effects are all included in the WRF-Chem simulation and analyzed separately. The WRF-Chem model configuration,

66 scenarios setup, and observation data are described in Section 2. Section 3 evaluates the model performance in simulating  
67 meteorology and air quality. In Section 4, the aerosol feedbacks on meteorology and air quality are analyzed and discussed.  
68 Section 5 investigates the effects of including aerosol feedbacks on the model performance. The concluding remarks are  
69 given in Section 6.

70 **2. Model and Observations Description**

71 **2.1 WRF-Chem Model and Scenarios Setup**

72 The WRF model is a state-of-the-art meso-scale non-hydrostatic model, and allows for many different choices for  
73 physical parameterizations (<http://www.wrf-model.org/>). WRF-Chem is a chemical version of WRF that simultaneously  
74 simulates meteorological and chemical components. The version 3.3 of WRF-Chem released on April 6, 2011 is used in this  
75 study. A more detailed description of the model can be found in previous studies (Grell et al., 2005; Fast et al., 2006;  
76 Chapman et al., 2009).

77 The main physical options selected in this study include the Goddard shortwave radiation scheme coupled with aerosol  
78 direct effects (Chou et al., 1998), the Rapid Radiative Transfer Model (RRTM) longwave radiation scheme (Mlawer et al.,  
79 1997), the Noah Land Surface Model (Chen and Dudhia, 2001), the Yonsei University (YSU) boundary layer scheme (Hong  
80 et al., 2006), the Lin microphysics scheme coupled with aerosol indirect effects (Lin et al., 1983), and the Grell-Devenyi  
81 cumulus parameterization scheme (Grell and D év ényi, 2002).

82 For the aerosol direct effect, aerosol optical properties such as extinction, single scattering albedo, and asymmetry  
83 factor are calculated as a function of wavelength and three-dimensional position, and then transferred to Goddard shortwave  
84 scheme. Mie theory is used to estimate the extinction efficiency. In this study, refractive indices are calculated based upon a  
85 volume-averaging approximation. The first and second indirect effects are implemented in the model (Gustafson et al., 2007;  
86 Chapman et al., 2009). Activated aerosols serving as CCN are coupled with cloud microphysics. Activation of aerosols  
87 follows the method of Ghan and Easter (2006), which is derived from Abdul-Razzak and Ghan (2002). Through this  
88 coupling, aerosols alter cloud droplet number and cloud radiative properties, while aqueous processes and wet scavenging  
89 also affect aerosols. In the model, aerosols change vertical profiles of meteorological variables by absorbing and scattering  
90 solar radiation, and further alter cumulus parameterization. When indirect effects are included, a more comprehensive in-  
91 and below-cloud aerosol wet removal module following the method of Easter et al (2004) is employed.

92 The Carbon Bond Mechanism version Z (CBMZ) (Zaveri and Peters, 1999) is used as the gas-phase chemistry scheme.  
93 The Model for Simulating Aerosol Interactions and Chemistry (MOSAIC) (Zaveri et al., 2008) is applied as aerosol module.  
94 MOSAIC simulates aerosol species including sulfate, methanesulfonate, nitrate, ammonium, chloride, carbonate, sodium,  
95 calcium, black carbon (BC), organic carbon (OC), and other unspecified inorganic matter (OIN). Secondary organic  
96 aerosols (SOA) are not included in the version of MOSAIC used in this study. Section 3.3 discusses the impact of SOA on  
97 our analysis by replacing MOSAIC with the Modal Aerosol Dynamics Model for Europe (MADE) (Ackermann et al., 1998)  
98 with the secondary organic aerosol model (SORGAM) (Schell et al., 2001) (referred to as MADE/SORGAM). MOSAIC in

99 WRF-Chem uses a sectional approach to represent particle size distribution. In this study, four size bins (0.039–0.156  $\mu\text{m}$ ,  
100 0.156–0.625  $\mu\text{m}$ , 0.625–2.5  $\mu\text{m}$ , 2.5–10.0  $\mu\text{m}$  dry diameter) are employed, and aerosols are assumed to be internally mixed  
101 within each bin.

102 The simulated time period is the whole month of January 2013. Figure 1 illustrates the model domain, which covers  
103 eastern China (19°–51°N, 96°–132°E) and has a horizontal resolution of 27 km  $\times$  27 km. There are 28 vertical levels  
104 extending from the surface to 50 hPa. The initial and boundary conditions for WRF are provided by the 6-hourly  $1^\circ \times 1^\circ$   
105 National Centers for Environmental Prediction (NCEP) Final Analysis (FNL). Chemical boundary conditions are provided  
106 by MOZART simulations (Emmons et al., 2010). In the initial spin-up process, the model is run with NCEP meteorological  
107 and MOZART chemical conditions for 48 hours, which are sufficient for the meteorological and chemical variables to reach  
108 equilibrium. Considering both accuracy and efficiency, the model's meteorology is re-initialized every five days based on  
109 NCEP, while chemistry adopts the previous state.

110 In order to investigate the impact of aerosol feedbacks on meteorology and air quality, three WRF-Chem simulation  
111 scenarios are performed and compared. The first is the baseline scenario (BASE), including all aerosol effects on  
112 meteorology (i.e., direct, indirect, and semi-direct). The second scenario (RAD) focuses on the radiative effects by  
113 excluding aerosol indirect effects from the BASE scenario. The third scenario (EMP) does not contain any aerosol effects  
114 on meteorology. Aerosol radiative properties are connected with the shortwave radiation scheme in the BASE and RAD  
115 scenario but not in the EMP scenario. Cloud droplet number is prescribed to be  $1.0 \times 10^6 / \text{kg}$  in EMP and RAD, while it is  
116 calculated based on aerosol activation in BASE. Other than the differences in aerosols effects, the three scenarios are  
117 identical in input data (e.g., emissions and boundary conditions) and model setup. The difference between BASE and EMP  
118 (i.e., BASE – EMP) is used to investigate the impact of total aerosol feedbacks, while the difference between BASE and  
119 RAD (i.e., BASE – RAD) and that between RAD and EMP (i.e., RAD – EMP) represents the influence of aerosol indirect  
120 effects and radiative (both direct and semi-direct) effects, respectively. Table 1 summaries the characteristics of the three  
121 scenarios.

## 122 **2.2 Emissions**

123 Anthropogenic emissions are taken from the Multi-resolution Emission Inventory of China (MEIC)  
124 (<http://www.meicmodel.org/>), which provides emissions of sulfur dioxide (SO<sub>2</sub>), nitrogen oxides (NO<sub>x</sub>), carbon monoxide  
125 (CO), ammonia (NH<sub>3</sub>), BC, OC, PM<sub>10</sub>, PM<sub>2.5</sub>, and non-methane volatile organic compounds (NMVOCs) for China for the  
126 year 2010. NO<sub>x</sub> emissions contain 90% of NO<sub>2</sub> and 10% of NO by mole fraction. PM emissions are assumed to be split into  
127 20% in nuclei mode and 80% in accumulation mode, according to the recommended construction of anthropogenic  
128 emissions inventory in WRF-Chem user's guide.

129 Biogenic emissions are calculated on-line in the model based on the Model of Emissions of Gases and Aerosols from  
130 Nature (MEGAN) inventory (Guenther et al., 2006). Dust is included in the simulations, while sea salt or dimethylsulfide  
131 (DMS) are not, and their impacts are expected to be small over eastern China in winter.

132 **2.3 Observations**

133 The simulation results are compared with meteorological and chemical observations. Daily meteorological  
134 observations at 523 stations are obtained from the National Climate Data Center (NCDC) of China Meteorological  
135 Administration (CMA), including 2 m temperature, 2 m relative humidity (RH), and 10 m wind speed. The radiosonde  
136 profiles at 20 stations are provided by the department of atmospheric science at the University of Wyoming  
137 (<http://weather.uwyo.edu/upperair/sounding.html>).

138 The measurements of near surface  $PM_{2.5}$  mass concentrations are obtained from China National Environmental  
139 Monitoring Center (CNEMC). The observation data have been released since January 2013, including hourly concentrations  
140 of  $SO_2$ ,  $NO_2$ , CO, Ozone ( $O_3$ ),  $PM_{10}$  and  $PM_{2.5}$  at 74 big cities in China with 71 of those cities covered by the study domain.  
141 Each city has several observation stations, containing both urban and rural stations. In this study, the  $PM_{2.5}$  concentration for  
142 one city is the average of all the stations in the city, representing thus a more regional condition of the pollution level. This  
143 database allows for a spatially extensive evaluation of air quality simulations by atmospheric models.

144 **3. Model Evaluations**

145 Accurate representation of meteorology and aerosol concentrations in the model provides the foundations of  
146 quantifying aerosol feedbacks. Therefore, in this section, the model performance is evaluated by comparing model results  
147 with surface and radiosonde observations. If not otherwise specified, the model results presented in this section are from the  
148 BASE scenario, which represents the most comprehensive realization of different processes in the model. It should be noted  
149 that systematic differences may result from the comparison between grid-mean values and point measurements, since a  
150 model grid covers an area of  $729 \text{ km}^2$  ( $27 \text{ km} \times 27 \text{ km}$ ).

151 **3.1 Meteorology**

152 Meteorology strongly affects formation, transport, and elimination of atmospheric aerosols. The selected  
153 meteorological variables for model evaluation are temperature, relative humidity, and wind speed. Figure 2 shows the time  
154 series of observed and simulated daily mean 2 m temperature and 2 m relative humidity, with the statistical summary of the  
155 comparisons shown in Table 2. The model reproduces temporal variations of these two meteorological variables.

156 The statistical indices used here are mean observation (MEAN OBS), mean simulation (MEAN SIM), correlation  
157 coefficient (Corr. R), mean bias (MB), normalized mean bias (NMB), and root mean square error (RMSE). The definitions  
158 of these indices are given in the Appendix. The model reproduces 2 m temperature with a correlation of 0.97 and a cold bias  
159 of  $-1.0 \text{ }^{\circ}\text{C}$ , mainly due to underestimation in the first 9 days of the month. Relative humidity is simulated with a correlation  
160 of 0.47 and a negligible mean bias. The 10 m wind speed is systematically overestimated by the model by 105%. A high  
161 positive bias in wind speed is also reported by several other studies using WRF-Chem (Matsui et al., 2009; Molders et al.,  
162 2012; Tuccella et al., 2012; Zhang et al., 2010). This high-bias probably results from unresolved topographical features in  
163 surface drag parameterization and the coarse resolution of the domain (Cheng and Steenburgh, 2005; Yahya et al., 2014).

164 Air pollution is influenced not only by surface meteorology, but also by vertical patterns of meteorological variables.

165 In Figure 3, the monthly mean vertical profiles of simulated meteorological variables are compared with sounding  
166 observations (averaged at 00UTC and 12UTC). Generally, the model captures vertical variations of meteorological variables.  
167 The model well reproduces vertical variations of temperature with a small bias. The model underestimates relative humidity  
168 below 650 hPa and overestimates it in the upper levels. Wind speeds are overestimated in the lower atmosphere and  
169 underestimated in the upper atmosphere. The errors in meteorology may influence the accuracy of simulating processes of  
170 aerosol formation, transport and deposition. Overall, the evaluations presented here suggest that the model adequately  
171 simulates the spatial and temporal variations of meteorological variables of significant relevance to air quality.

### 172 3.2 PM<sub>2.5</sub>

173 We first evaluated the spatial distribution of simulated monthly mean PM<sub>2.5</sub> mass concentrations by comparing model  
174 results with observations at 71 big cities in the model domain in January 2013. As shown in Figure 4, the model captures the  
175 spatial patterns of PM<sub>2.5</sub> during the month, including high levels of PM<sub>2.5</sub> over southern Hebei, Henan, Hubei Province,  
176 Sichuan Basin and three big cities (Harbin, Changchun, Shenyang) in Northeast China. The North China Plain (NCP),  
177 Central China (CC) area, and Sichuan Basin have the highest monthly mean PM<sub>2.5</sub> mass concentrations. PM<sub>2.5</sub> pollution is  
178 more severe over the Yangtze River Delta (YRD) than that over the Pearl River Delta (PRD).

179 Figure 5 presents the scatter plots of observed and simulated monthly mean PM<sub>2.5</sub> mass concentrations at 71 cities. The  
180 model has a low bias ranging from 25% to 70% for cities with monthly mean PM<sub>2.5</sub> exceeding 200  $\mu\text{g}/\text{m}^3$ . The observed and  
181 simulated time-series of hourly surface PM<sub>2.5</sub> averaged over all the cities are compared in Figure 6. The model simulates  
182 hourly PM<sub>2.5</sub> with a temporal correlation of 0.67, and underestimates monthly mean PM<sub>2.5</sub> mass concentrations by 18.9  
183  $\mu\text{g}/\text{m}^3$  (15.0%). The model generally reproduces the observed temporal variations of PM<sub>2.5</sub>.

184 The enhancement ratio is employed to further evaluate the model performance in simulating PM<sub>2.5</sub> temporal variations  
185 in different regions. Within a given grid point, the enhancement ratio is defined as the average of daily PM<sub>2.5</sub> mass  
186 concentrations exceeding the median divided by that less than the median, representing changes of PM<sub>2.5</sub> from clean to  
187 polluted situations. As shown in Table 3, observed enhancement ratios are around 1.6 over NCP, YRD, PRD and CC. The  
188 simulated enhancement ratios range from 1.8 to 2.0 over the four regions, which are close to observations. Since changes of  
189 hourly emissions are not considered in this study, PM<sub>2.5</sub> enhancements mainly result from worsened meteorological  
190 conditions and more production of secondary aerosols. The consistency of the simulated enhancement ratios with the  
191 observed ones by region indicates that the WRF-Chem model has some success in simulating the changes of meteorological  
192 and chemical processes from clean to polluted situations.

193 However, the model fails to capture the extremely high values of PM<sub>2.5</sub> during the haze episodes in January 2013, for  
194 example, January 13~15 and 18~20. Both positive and negative bias exists in simulated hourly PM<sub>2.5</sub>. The model's  
195 underestimation during the severe winter haze episodes is consistent with previous studies (Liu et al., 2010; Wang, L. T. et  
196 al., 2014; Wang, Y. X. et al., 2014; Zhou et al., 2014). Possible reasons for this underestimation are: (1) the bias in  
197 simulating meteorological conditions during haze episodes; (2) uncertainties in emissions; (3) missing SOA in the MOS AIC

198 mechanism, which will be addressed below; and (4) the lack of formation mechanisms of secondary inorganic aerosols, like  
199 heterogeneous oxidation of  $\text{SO}_2$  on the surface of particulate matter (Harris et al., 2013). By adjusting  $\text{SO}_2$  and  $\text{NO}_x$   
200 emissions according to surface observations and parameterizing the heterogeneous oxidation of  $\text{SO}_2$  on deliquesced aerosols  
201 in the GEOS-Chem model, Wang, Y. X. et al (2014) reported improvements of simulated  $\text{PM}_{2.5}$  spatial distribution and an  
202 increase of 120% in sulfate fraction in  $\text{PM}_{2.5}$ . The traditional offline models do not include the aerosol feedbacks on  
203 meteorology, which may cause a low-bias of  $\text{PM}_{2.5}$  for the severe pollution episodes. The inclusion of aerosol feedbacks in  
204 atmospheric models improves the model performance, which will be discussed in Section 5.

### 205 3.3 SOA

206 The MOSAIC aerosol module used in the three scenarios does not include SOA. Here we examine the sensitivity of  
207 modeled  $\text{PM}_{2.5}$  to SOA by replacing MOSAIC with the MADE/SORGAM aerosol module in the BASE scenario. The test  
208 period is January 6~10, 2013. The mean SOA simulated from MADE/SORGAM is  $0.3 \text{ ug/m}^3$ , making up only 2.8% of OA  
209 (Table 4). This is comparable with the magnitude of simulated winter SOA concentrations reported by another study using  
210 WRF-Chem for the whole China (Jiang et al., 2012). The low SOA concentrations simulated by the model can be explained  
211 by low emissions of biogenic VOCs (key precursors of SOA) and low temperatures in wintertime. Recent observations have  
212 suggested much higher SOA concentrations at Chinese cities in winter, pointing to the importance of anthropogenic VOCs  
213 as SOA precursors in China (Huang et al., 2014), but a thorough investigation of this issue is outside the scope of this study.  
214 As shown in Table 4, the NMB of  $\text{PM}_{2.5}$  with the MADE/SORGAM option is more than 3 times larger than that with  
215 MOSAIC. Since the modeled SOA has a small contribution to total  $\text{PM}_{2.5}$ , the MOSAIC aerosol module is chosen in this  
216 study and the omission of SOA in MOSAIC is not expected to affect our analysis of the aerosol effects on meteorology.

## 217 4. Aerosol Feedbacks on Meteorology and Air Quality

218 As seen in the previous section, the WRF-Chem model has shown some success in simulating meteorology and  $\text{PM}_{2.5}$ .  
219 Therefore, in this section, we aim to characterize and quantify the aerosol feedbacks on meteorology and air quality by  
220 comparing the three different scenarios described in Section 2.

221 In addition to different setups of the aerosol-radiation-cloud feedbacks, differences among the three scenarios can also  
222 result from model noise, such as errors in numerical computation and disturbances from discrete updating initial and  
223 boundary conditions. The Student's t-test is employed to identify statistically significant differences between the scenarios.  
224 The null hypothesis is that the two scenarios in comparison give the same simulation results. The sample size is 744 (24 hrs  
225  $\times$  31 days) for each meteorological and chemical variable in a given grid box. Rejection of the null hypothesis indicates that  
226 the difference between the two scenarios is significantly different. The Appendix describes the calculation of the t statistic in  
227 more detail. We only present and discuss aerosol-induced changes of meteorological and chemical variables which exceed  
228 95% confidence interval.

### 229 4.1 Feedbacks on Meteorology

230 The evolution of atmospheric aerosols is strongly influenced by meteorological variables, such as solar radiation, air

temperature, and wind speed. Figure 7 illustrates the mean impact of aerosols on downward shortwave flux at the ground, 2 m temperature, 10 m wind speed and PBL height over eastern China in January 2013. Downward shortwave flux at the ground is strongly influenced by the existence of atmospheric aerosols, especially over high aerosol-loading regions. Aerosols affect shortwave radiation reaching the ground in two ways. First, particles scatter and absorb incoming solar radiation directly, resulting in surface dimming. Second, in-cloud particles change cloud lifetime and albedo, thus causing variations of shortwave radiation at the ground surface. As in Figure 7a, the downward shortwave flux at the ground is reduced over the vast areas of eastern China by up to  $-84.0 \text{ W/m}^2$ , which mainly results from the aerosol radiative effects (Figure 7b). Consistent with our findings, Bi et al (2014) and Che et al (2014) report strong negative aerosol direct radiative forcing at the surface (with maximum daily mean exceeding  $-200.0 \text{ W/m}^2$ ) through analysis of ground-based measurements, aerosol optical and radiative properties over NCP in January 2013.

When the downward shortwave flux at the ground is decreased due to aerosol interception, near surface energy fluxes are suppressed, leading to weaker convection. Near surface air is heated mainly by longwave radiation emitted from the ground. In the case of decreasing shortwave flux at the ground, the near surface air is cooled and less longwave radiation is emitted from the surface. Due to weaker convection resulting from less shortwave radiation reaching the ground, 2 m temperature is reduced by up to  $3.2 \text{ }^\circ\text{C}$ , 10 m wind speed is reduced by up to 0.8 m/s, and PBL height is also reduced by up to 268 m, as shown in Figure 7c, 7e and 7g, respectively. Meteorological variables such as air temperature, wind speed, and PBL height could also be influenced by other factors like land surface properties (Zhang et al., 2010), in addition to solar radiations. The change of these variables, especially wind speed, is less significant than that of solar radiation. First, solar radiation is reduced by 21% over the regions with significant changes, while wind speed and PBL height are reduced by 6% and 14%, respectively. Second, as shown by Figure 7, the regions with significant reduced solar radiation are much larger than those with significant reduced wind speed or PBL height. However, the spatial pattern of the changes of these variables is consistent with that of downward shortwave flux, which indicates that a more stable lower atmosphere resulting from less shortwave radiation plays an important role in aerosol feedbacks. The aerosol indirect effects during the severe haze episodes are found to be not significant in altering solar radiation, temperature, wind speed or PBL height over eastern China, which is not shown here. Overall, the near surface atmosphere is more stable when aerosol feedback is considered in the model, which enhances pollution accumulation.

The amount of precipitation is low in January 2013 for most regions in China (Wang and Zhou, 2005). Cloud and precipitation formation mainly occurs over areas in the south and over the ocean (Figure 8a and 8d). In this month, the changes of cloud and precipitation due to aerosol radiative effects are not significant (Figure 8h). Aerosol indirect effects directly alter cloud properties such as effective radius, cloud lifetime, and precipitation rate. As shown in Figure 8i, aerosol indirect effects play a much more significant role in changing cloud properties, mostly in the south. Cloud water path is greatly reduced by up to  $5.7 \text{ kg/m}^2$  over the junction of Yunnan and Guizhou Province and the ocean around Taiwan. The reduction over these relatively clean areas may be explained by the smaller droplet number mixing ratio which is derived

from lower particle number concentrations in the BASE scenario. The scenarios without aerosol indirect effects adopt the default value droplet number mixing ratio of  $1.0 \times 10^6$  /kg which does not vary with aerosol number concentrations. Reduced cloud droplet number results in accelerating auto-conversion to rain droplets. Thus, simulated monthly precipitation is increased by almost 100% over these areas (Figure 8j). Similar results are found when we replace the Lin microphysics scheme by the two-moment Morrison scheme (Morrison et al., 2009). Previous model assessments also showed that the inclusion of aerosol indirect effect reduced cloud water content over South Pacific ocean and improved model comparison with aircraft observations (Yang et al., 2011). The relatively small precipitation, as well as small changes of precipitation due to aerosol feedbacks over the north of the domain, suggests that precipitation has a minor effect on near surface aerosols in January 2013.

Several studies under the Air Quality Model Evaluation International Initiative (AQMEII) project suggested that the aerosol indirect effect dominated in aerosol feedbacks on solar radiation, temperature, and PBL height (Forkel et al., 2012; Forkel et al., 2014; Kong et al., 2014; Makar et al., 2014a). Different from these studies, we find that aerosol indirect effects have little influence on the downward shortwave flux at the ground, 2 m temperature, 10 m wind speed, and PBL height (not shown here). In order to investigate how grid resolution relates to aerosol indirect effect, we have conducted another three groups of nested grid runs, using the same scenarios (BASE, RAD, and EMP). The outer domain is the same with previous domain, but a 9-km nested domain covering North China Plain is added. In the nested domain, cumulus parameterization is turned off. We find that with the finer resolution simulation, aerosol direct effect still dominates over NCP and aerosol indirect effect is not significant, suggesting grid resolution might not be the reason why aerosol indirect effect is minor in our study.

The discrepancy relating to aerosol indirect effect between those studies under AQMEII and our work may be explained by three reasons. First, we focus on a low-cloud-cover winter case, especially in North China. It is confirmed by both the more sophisticated Morrison scheme and the finer resolution (9-km) nested grid simulation that cloud cover is low in North China. Studies under AQMEII focused on summertime, when aerosol indirect effects on solar radiation, temperature, and PBL height were found to be most pronounced (Forkel et al., 2014). Second, under high aerosol loading conditions (for example, fire conditions in Kong et al (2014) and haze conditions in our study), aerosol direct effect is found to dominate over aerosol indirect effect. The aerosol indirect effect was found to dominate over clean ocean and near ocean land (Forkel et al., 2014; Kong et al., 2014). Third, we do find some regions dominated by aerosol indirect effect. However, the Student's t test filters the values over those regions, because the changes due to aerosol indirect effect are not statistically significant.

Ice crystals can be formed by activation of Ice Nuclei (IN). Recently, increasing evidence has suggested that aerosols, especially dust, black carbon, and organic matters, can influence cloud physical process by acting as IN (Tao et al., 2012). The WRF-Chem version in this work does not include direct interactions of aerosol number concentration with ice nuclei, which may be another reason for the possible underestimation of aerosol indirect effects.

297 **4.2 Feedbacks on Air Quality**

298 Through moderating meteorological variables, aerosols exert feedbacks on air quality. Figure 9 shows spatial  
299 distributions of CO, SO<sub>2</sub>, and O<sub>3</sub> and the feedbacks of aerosols on these three gas pollutants in January 2013. Spatial  
300 patterns of CO and SO<sub>2</sub> are similar with that of PM<sub>2.5</sub>. The near surface CO and SO<sub>2</sub> concentrations are increased when  
301 aerosol feedbacks are included. Over the domain, CO is enhanced by up to 446 ppb, while SO<sub>2</sub> is increased by as much as  
302 28 ppb. Large increases of CO and SO<sub>2</sub> are found over areas with high aerosol loading. This phenomenon may mainly result  
303 from lower PBL and a more stable atmosphere near the surface due to aerosol radiative effects, as discussed in Section 3.2.  
304 We also found aerosol indirect effects do not have significant influence on gas pollutants.

305 The formation of O<sub>3</sub> is directly related to solar radiation and temperature in regions with sufficient NO<sub>x</sub> and VOCs. The  
306 lower air temperature and reduced incoming solar radiation as a result of aerosols radiative effects lead to reduced  
307 photolysis rate of NO<sub>2</sub> and consequently reduce O<sub>3</sub> concentrations. The largest suppression of surface ozone by aerosols is  
308 found to be up to -6.9 ppb in the warmer southern China. Changes in northern China are relatively small. These findings are  
309 similar to those in Zhang et al (2010), Forkel et al (2012), Kong et al (2014) and Makar et al (2014b).

310 The aerosol-radiation-cloud feedbacks on near surface aerosol mass concentrations are illustrated in Figure 10. As  
311 shown in Figure 10a, both increases and decreases of PM<sub>2.5</sub> are found in the domain. Enhanced PM<sub>2.5</sub> mass concentrations  
312 are simulated over Henan, Hubei, Guangxi Province, and Sichuan Basin with the maximum enhancement of 69.3  $\mu\text{g}/\text{m}^3$ .  
313 Reductions in PM<sub>2.5</sub> as much as -38.2  $\mu\text{g}/\text{m}^3$  are simulated over the Bohai Sea surrounding area, Northeast China and the  
314 conjunction area of Yunnan, Guangxi, and Guizhou Province (Southwest China).

315 In order to better understand the mechanisms of how PM<sub>2.5</sub> responds to aerosol feedbacks, the aerosol effects are  
316 divided into aerosol radiative effects (Figure 10b) and indirect effects (Figure 10c). PM<sub>2.5</sub> can be influenced by the changes  
317 in various atmospheric processes due to aerosol radiative effects. For example, lower temperature may suppress the  
318 formation of sulfate, and reduced solar radiation may inhibit the oxidations of precursors of secondary aerosols. Among the  
319 various changes in atmospheric processes, the reduced PBL height and the stabilized lower atmosphere may be the most  
320 important factors to explain the increase of PM<sub>2.5</sub> caused by the aerosol radiative effects, since primary gas pollutants also  
321 increase when aerosol radiative effects are included. From Figure 11b, we can see that PM<sub>2.5</sub> is greatly increased by aerosol  
322 radiative effects over the region where solar radiation and PBL height are significantly reduced during winter haze (Figure  
323 7a and 7g). The mechanism involved is that aerosol radiative effects stabilize the lower atmosphere and suppress the  
324 dilution and ventilation of PM<sub>2.5</sub> as well as primary gas pollutants.

325 The comparison between Figure 10a and 10c indicates that aerosol indirect effects are the main reason of the  
326 suppression of PM<sub>2.5</sub>. The reduction of PM<sub>2.5</sub> in WRF-Chem simulations with aerosol indirect effects mainly comes from  
327 three aspects. First, once aerosol indirect effects are included in the model, the cloud droplet number is based on simulated  
328 atmospheric aerosol number other than what is prescribed in the model. This coding strategy allows interstitial air-borne  
329 aerosols to become cloud-borne aerosols after activation. Therefore, air-borne aerosols are reduced in simulations including

aerosol indirect effects, especially over cloudy regions like southwestern China (Figure 8a). Second, enhanced precipitation may also help reduce the air-borne particles, especially in the south. Third, in the simulations including aerosol indirect effects, a more comprehensive in- and below-cloud aerosol wet removal module following the method of Easter et al (2004) is employed, while in the simulations without aerosol indirect effects, this module is not activated. In this aerosol wet removal mechanism, the removal processes are assumed to be irreversible, and aerosol re-suspension is not considered, even when precipitation is weak. This leads to a stronger removal of atmospheric aerosols when aerosol indirect effects are included. It should be noted that in this work, the enhancement of aerosol wet removal process, when including aerosol indirect effects in the model, mainly results from WRF-Chem model configurations used here, not from aerosol-induced changes in cloud properties or precipitation.

The above discussion is based on model results temporally averaged during the whole month. In order to better understand PM<sub>2.5</sub> variations on a day to day basis, 4 cities with significant PM<sub>2.5</sub> enhancements and 4 cities with significant PM<sub>2.5</sub> reductions are selected. Figure 11 shows the time series of observed and simulated hourly surface PM<sub>2.5</sub> mass concentrations in the selected 8 cities in January 2013. The four cities with increasing monthly mean PM<sub>2.5</sub> due to aerosol feedbacks are Zhengzhou, Wuhan, Changsha, and Chengdu (left panels in Figure 11). Major enhancements of PM<sub>2.5</sub> are simulated when PM<sub>2.5</sub> levels are high, for example, during the period of January 15~17. The changes in PM<sub>2.5</sub> have a moderate negative correlation with the changes in PBL height (correlation coefficient  $\approx -0.3$ ) at the four cities, suggesting that the PM<sub>2.5</sub> enhancement is partly caused by decreased PBL height in these regions. The reduction of PM<sub>2.5</sub> in Qinhuangdao, Tianjin, Shenyang, and Changchun (right panels in Figure 11), which are the four cities with decreased monthly mean PM<sub>2.5</sub>, mainly happens in the last 5 days of the month (January 26~31).

In summary, aerosol radiative effects reduce the downward shortwave flux at the ground, decrease near surface temperature and wind speed, and further weaken convection, all leading to a more stable lower atmosphere. In a more stable lower atmosphere due to aerosol radiative effects, primary gas pollutants (CO and SO<sub>2</sub>) and PM<sub>2.5</sub> are enhanced, while O<sub>3</sub> is decreased because of less incoming solar radiation and lower temperatures. PM<sub>2.5</sub> is reduced when aerosol indirect effects are included, mainly due to the transition from air-borne aerosol to cloud-borne aerosol and the activation of a more comprehensive aerosol wet removal module. The underestimations at the higher end indicate that some key mechanisms are missing in the model, especially the production of secondary aerosols.

## 356 **5. Effects of Including Aerosol Feedbacks on Model Performance**

357 In this section we address the question whether including aerosol feedbacks within the model improves model  
358 performance in simulating severe haze episodes. Model results from the BASE (with all aerosol feedbacks) and EMP  
359 (without any aerosol feedbacks) scenarios are compared with observations to evaluate which scenario is more consistent  
360 with reality.

361 As an example to show the extent to which simulated meteorological variables are affected by including aerosol  
362 feedbacks, Figure 12 compares downward shortwave radiation at the ground and 2 m temperature among the three scenarios

363 over NCP, where  $PM_{2.5}$  pollution is most severe in January 2013. All scenarios have a high bias in daily total shortwave  
364 radiation at the ground, mainly due to the overestimation of maximum shortwave radiation at noon (Wang, Z. F. et al., 2014).  
365 However, the inclusion of all aerosol feedbacks (BASE) leads to a 22% reduction of the normalized mean bias. Simulated  
366 shortwave radiation in the RAD scenario has the smallest bias. The model prediction of 2 m temperature is also improved in  
367 the scenario with aerosol feedbacks during haze episodes, such like January 12~15 and 19~24. These findings are consistent  
368 with the those from Wang, Z. F. et al (2014), indicating the importance of including aerosol feedbacks in simulating  
369 meteorology under high aerosol loading conditions.

370 Figure 5 and Figure 6 compare simulated  $PM_{2.5}$  over 71 big cities in January 2013 in the BASE and EMP scenarios  
371 averaged temporally and spatially, respectively. However, no significant improvements are found when aerosol feedbacks  
372 are included, partially due to temporal and spatial averaging. So we further investigate the model performance in simulating  
373  $PM_{2.5}$  over several important regions. Box plots of monthly mean  $PM_{2.5}$  mass concentrations in January 2013 over NCP,  
374 YRD, PRD and CC are displayed in Figure 13. Over all the four regions, the median values of hourly  $PM_{2.5}$  are  
375 underestimated in the EMP scenario, in which aerosol feedbacks are excluded. Biases of the median values in the EMP  
376 scenario are  $-29.1\%$ ,  $-16.8\%$ ,  $-10.7\%$ ,  $-5.3\%$  over NCP, YRD, PRD, and CC, respectively. Through including aerosol  
377 feedbacks, the BASE scenario improves the simulation of hourly  $PM_{2.5}$  mass concentrations in two aspects. First, biases of  
378 the median values are reduced to  $-22.0\%$ ,  $-12.0\%$ ,  $-6.7\%$ ,  $+2.6\%$  over NCP, YRD, PRD, and CC, respectively. Second, the  
379 distribution of the middle 50% (ranging from 25<sup>th</sup> percentile to 75<sup>th</sup> percentile) hourly  $PM_{2.5}$  mass concentrations is more  
380 consistent with observations than without aerosol feedbacks in the model. We also find a positive feedback for  $PM_{2.5}$ ; that is,  
381 aerosols increase  $PM_{2.5}$  through meteorological and chemical processes.

382 Overall in this section, we demonstrate the significance of including aerosol feedbacks in the model. Inclusions of  
383 aerosol feedbacks in the model reproduce aerosol effects on solar radiation and temperature. Thus, biases of simulated  
384 meteorology are reduced. Though the responses of  $PM_{2.5}$  to aerosol feedbacks are complex, the inclusion of aerosol  
385 feedbacks improves the model performance to some extent in simulating  $PM_{2.5}$  in winter haze conditions.

## 386 6. Conclusions

387 In this work, the fully coupled on-line WRF-Chem model is applied to investigate aerosol-radiation-cloud feedbacks  
388 on meteorology and air quality over eastern China in January 2013, in which month China experienced the most severe haze  
389 pollution in history. Three simulation scenarios including different aerosol configurations are undertaken and compared.

390 The evaluation of the baseline simulation shows that the model captures temporal and vertical variations of  
391 meteorological variables, except for overestimating lower atmosphere wind speed which is a common issue for the  
392 WRF-Chem model. The model reproduces spatial distribution of monthly mean  $PM_{2.5}$  mass concentration, with high aerosol  
393 concentrations over southern Hebei, Henan, Hubei Province, Sichuan Basin and three big cities (Harbin, Changchun,  
394 Shenyang) in Northeast China. Monthly mean  $PM_{2.5}$  averaged over 71 big cities is underestimated by 15%. The model tends  
395 to underestimate  $PM_{2.5}$  at the high ends, which is a common problem for current models in simulating severe haze

396 conditions. Further studies are needed to improve model abilities in simulating high aerosol pollution.

397 Previous work indicated that the influences on air quality meteorology of aerosol indirect effects are larger than  
398 radiative effects, but this was derived under conditions with much lower aerosol loadings than those in our study. In this  
399 work we find that under winter haze conditions, aerosol radiative effects (direct effect and semi-direct effects) play a  
400 dominant role in modulating downward shortwave flux at the ground surface, lower atmosphere temperature, wind speed  
401 and PBL height. These four meteorological variables are reduced by up to  $84.0 \text{ W/m}^2$ ,  $3.2 \text{ }^\circ\text{C}$ ,  $0.8 \text{ m/s}$ , and  $268 \text{ m}$ ,  
402 respectively. However, aerosol indirect effects are more important than radiative effects in altering cloud properties and  
403 precipitation.

404 The lower PBL and stabilized lower atmosphere result in increases of near surface CO and  $\text{SO}_2$  concentrations. Higher  
405 aerosol loading reduces solar radiation and temperature at the surface, which results in a reduction of  $\text{NO}_2$  photolysis rate  
406 and subsequently a reduction in a reduction of  $\text{O}_3$  mixing ratios by up to  $6.9 \text{ ppb}$ . The aerosol feedbacks on  $\text{PM}_{2.5}$   
407 concentrations exhibit large spatial variations. Both increases and decreases of  $\text{PM}_{2.5}$  are found in the domain. The  
408 enhancements of  $\text{PM}_{2.5}$  over Henan, Hubei Province, and Sichuan Basin by up to  $17.8 \text{ } \mu\text{g/m}^3$  are mainly due to large  
409 reduction of PBL height in these areas. The reduction of  $\text{PM}_{2.5}$  over Bohai Sea surrounding area, Northeast China, and  
410 Southwestern China are resulted from the transition from air-borne aerosol to cloud-borne aerosol and the activation of a  
411 more comprehensive aerosol wet removal module.

412 The inclusion of aerosol feedback improves the model's ability in simulating downward shortwave radiation and  
413 temperature. Simulations of hourly  $\text{PM}_{2.5}$  mass concentration distributions over NCP, YRD, PRD, and CC, are also  
414 improved when aerosol feedbacks are included. These indicate the importance of involving aerosol-radiation-cloud  
415 interactions in modeling air quality meteorology.

416 There are a number of limitations in this work. The relative coarse grid (27 km), the uncertainty of emission inventory,  
417 and the lack of secondary organic matters all contribute to the uncertainties in simulating aerosols. Also, one month length  
418 simulation could not represent a full view of aerosol-radiation-cloud feedbacks. Better understandings in the future are  
419 expected by applying more comprehensive aerosol treatments and a longer time period. Previous studies mainly focus on  
420 mechanisms of severe winter haze formation. Different from them, this work demonstrates the importance of aerosol  
421 feedbacks on meteorology and air quality during severe winter haze periods.

422  
423 **Acknowledgement:** This research was supported by the National Key Basic Research Program of China (2014CB441302),  
424 the CAS Strategic Priority Research Program (Grant No. XDA05100403), and the Beijing Nova Program  
425 (Z121109002512052).

426  
427 **Appendix**

428 The statistical indices used in this study are defined as following.

429 (1) Mean Bias (MB)

$$430 MB = 1/N \sum_{i=1}^N (M_i - O_i)$$

431 (2) Normalized Mean Bias (NMB)

$$432 NMB = \frac{\sum_{i=1}^N (M_i - O_i)}{\sum_{i=1}^N O_i} \times 100\%$$

433 (3) Correlation Coefficient (Corr. R)

$$434 Corr.R = \frac{\sum_{i=1}^N (M_i - \bar{M})(O_i - \bar{O})}{\sqrt{\sum_{i=1}^N (M_i - \bar{M})^2} \sqrt{\sum_{i=1}^N (O_i - \bar{O})^2}}$$

435 (4) Root Mean Square Error (RMSE)

$$436 RMSE = \sqrt{1/N \sum_{i=1}^N (M_i - O_i)^2}$$

437 where  $\bar{M} = 1/N \sum_{i=1}^N M_i$ ,  $\bar{O} = 1/N \sum_{i=1}^N O_i$ ,  $\bar{M}$  and  $\bar{O}$  are model result and observation for sample  $i$ , respectively.

438  $N$  is the number of samples.

439 (5) The Student t statistic

$$440 t = \frac{\bar{X}_1 - \bar{X}_2}{S_{X_1 X_2} \sqrt{1/n_1 + 1/n_2}}$$

$$441 S_{X_1 X_2} = \sqrt{\frac{(n_1 - 1)S_{X_1}^2 + (n_2 - 1)S_{X_2}^2}{n_1 + n_2 - 2}}$$

442 Here,  $S_{X_1 X_2}$  is the grand standard deviation,  $S_{X_1}^2$  and  $S_{X_2}^2$  are the variances of the two samples.

443

#### 444 References

445 Ackermann, I. J., Hass, H., Memmesheimer, M., Ebel, A., Binkowski, F. S., and Shankar, U.: Modal aerosol dynamics  
446 model for Europe: Development and first applications, *Atmospheric environment*, 32, 2981-2999, 1998.

447 Albrecht, B. A.: Aerosols, cloud microphysics, and fractional cloudiness, *Science*, 245, 1227-1230, 1989.

448 Bi, J., Huang, J., Hu, Z., Holben, B. N., and Guo, Z.: Investigate the aerosol optical and radiative characteristics of heavy  
449 haze episodes in Beijing during January of 2013, *Journal of Geophysical Research: Atmospheres*, 9884-9900,  
450 2014JD021757, 10.1002/2014JD021757, 2014.

451 Chapman, E. G., Gustafson Jr, W., Easter, R. C., Barnard, J. C., Ghan, S. J., Pekour, M. S., and Fast, J. D.: Coupling

452 aerosol-cloud-radiative processes in the WRF-Chem model: Investigating the radiative impact of elevated point  
453 sources, *Atmospheric Chemistry and Physics*, 9, 945-964, 2009.

454 Charlson, R., and Pilat, M.: Climate: The influence of aerosols, *Journal of Applied Meteorology*, 8, 1001-1002, 1969.

455 Che, H., Xia, X., Zhu, J., Li, Z., Dubovik, O., Holben, B., Goloub, P., Chen, H., Estelles, V., Cuevas-Agulló, E., Blarel, L.,  
456 Wang, H., Zhao, H., Zhang, X., Wang, Y., Sun, J., Tao, R., Zhang, X., and Shi, G.: Column aerosol optical properties  
457 and aerosol radiative forcing during a serious haze-fog month over North China Plain in 2013 based on ground-based  
458 sunphotometer measurements, *Atmos. Chem. Phys.*, 14, 2125-2138, 10.5194/acp-14-2125-2014, 2014.

459 Chen, F., and Dudhia, J.: Coupling an advanced land surface-hydrology model with the Penn State-NCAR MM5 modeling  
460 system. Part I: Model implementation and sensitivity, *Monthly Weather Review*, 129, 569-585, 2001.

461 Cheng, W. Y. Y., and Steenburgh, W. J.: Evaluation of Surface Sensible Weather Forecasts by the WRF and the Eta Models  
462 over the Western United States, *Weather and Forecasting*, 20, 812-821, doi:10.1175/WAF885.1, 2005.

463 Chou, M.-D., Suarez, M. J., Ho, C.-H., and Yan, M. M.-H.: Parameterizations for cloud overlapping and shortwave  
464 single-scattering properties for use in general circulation and cloud ensemble models, *Journal of climate*, 11, 202-214,  
465 doi:10.1175/1520-0442(1998)011<0202:PFCOAS>2.0.CO;2, 1998.

466 Emmons, L., Walters, S., Hess, P., Lamarque, J.-F., Pfister, G., Fillmore, D., Granier, C., Guenther, A., Kinnison, D., and  
467 Laepple, T.: Description and evaluation of the Model for Ozone and Related chemical Tracers, version 4 (MOZART-4),  
468 *Geoscientific Model Development*, 3, 43-67, 2010.

469 Fan, J., Zhang, R., Tao, W. K., and Mohr, K. I.: Effects of aerosol optical properties on deep convective clouds and radiative  
470 forcing, *Journal of Geophysical Research: Atmospheres* (1984–2012), 113, D08209, doi:10.1029/2007JD009257,  
471 2008.

472 Fast, J. D., Gustafson, W. I., Easter, R. C., Zaveri, R. A., Barnard, J. C., Chapman, E. G., Grell, G. A., and Peckham, S. E.:  
473 Evolution of ozone, particulates, and aerosol direct radiative forcing in the vicinity of Houston using a fully coupled  
474 meteorology - chemistry - aerosol model, *Journal of Geophysical Research: Atmospheres* (1984–2012), 111, D21305,  
475 doi:10.1029/2005JD006721, 2006.

476 Forkel, R., Werhahn, J., Hansen, A. B., McKeen, S., Peckham, S., Grell, G., and Suppan, P.: Effect of aerosol-radiation  
477 feedback on regional air quality—a case study with WRF/Chem, *Atmospheric environment*, 53, 202-211, 2012.

478 Forkel, R., Balzarini, A., Baró, R., Bianconi, R., Curci, G., Jiménez-Guerrero, P., Hirtl, M., Honzak, L., Lorenz, C., Im, U.,  
479 Pérez, J. L., Pirovano, G., San José, R., Tuccella, P., Werhahn, J., and Žabkar, R.: Analysis of the WRF-Chem  
480 contributions to AQMEII phase2 with respect to aerosol radiative feedbacks on meteorology and pollutant distributions,  
481 *Atmospheric Environment*, <http://dx.doi.org/10.1016/j.atmosenv.2014.10.056>, 2014.

482 Grell, G., and Baklanov, A.: Integrated modeling for forecasting weather and air quality: A call for fully coupled approaches,  
483 *Atmospheric Environment*, 45, 6845-6851, <http://dx.doi.org/10.1016/j.atmosenv.2011.01.017>, 2011.

484 Grell, G. A., and Dévényi, D.: A generalized approach to parameterizing convection combining ensemble and data

485 assimilation techniques, *Geophysical Research Letters*, 29, 38-31-38-34, 2002.

486 Grell, G. A., Peckham, S. E., Schmitz, R., McKeen, S. A., Frost, G., Skamarock, W. C., and Eder, B.: Fully coupled “online”  
487 chemistry within the WRF model, *Atmospheric Environment*, 39, 6957-6975, 2005.

488 Guenther, A., Karl, T., Harley, P., Wiedinmyer, C., Palmer, P., and Geron, C.: Estimates of global terrestrial isoprene  
489 emissions using MEGAN (Model of Emissions of Gases and Aerosols from Nature), *Atmospheric Chemistry &*  
490 *Physics*, 6, 2006.

491 Gustafson, W. I., Chapman, E. G., Ghan, S. J., Easter, R. C., and Fast, J. D.: Impact on modeled cloud characteristics due to  
492 simplified treatment of uniform cloud condensation nuclei during NEAQS 2004, *Geophysical Research Letters*, 34,  
493 L19809, 10.1029/2007GL030021, 2007.

494 Hansen, J., Sato, M., and Ruedy, R.: Radiative forcing and climate response, *Journal of Geophysical Research: Atmospheres*  
495 (1984–2012), 102, 6831-6864, 1997.

496 Harris, E., Sinha, B., van Pinxteren, D., Tilgner, A., Fomba, K. W., Schneider, J., Roth, A., Gnauk, T., Fahrbusch, B., and  
497 Mertes, S.: Enhanced role of transition metal ion catalysis during in-cloud oxidation of SO<sub>2</sub>, *science*, 340, 727-730,  
498 2013.

499 Hong, S.-Y., Noh, Y., and Dudhia, J.: A new vertical diffusion package with an explicit treatment of entrainment processes,  
500 *Monthly Weather Review*, 134, 2318-2341, doi: 10.1175/MWR3199.1, 2006.

501 Huang, K., Zhuang, G., Wang, Q., Fu, J. S., Lin, Y., Liu, T., Han, L., and Deng, C.: Extreme haze pollution in Beijing during  
502 January 2013: chemical characteristics, formation mechanism and role of fog processing, *Atmos. Chem. Phys. Discuss.*,  
503 14, 7517-7556, 10.5194/acpd-14-7517-2014, 2014.

504 Huang, R. J., Zhang, Y., Bozzetti, C., Ho, K. F., Cao, J. J., Han, Y., Daellenbach, K. R., Slowik, J. G., Platt, S. M., Canonaco,  
505 F., Zotter, P., Wolf, R., Pieber, S. M., Bruns, E. A., Crippa, M., Ciarelli, G., Piazzalunga, A., Schwikowski, M.,  
506 Abbaszade, G., Schnelle-Kreis, J., Zimmermann, R., An, Z., Szidat, S., Baltensperger, U., Haddad, I. E., and Prevot, A.  
507 S. H.: High secondary aerosol contribution to particulate pollution during haze events in China, *Nature*, 514, 218-222,  
508 10.1038/nature13774, 2014.

509 Jiang, F., Liu, Q., Huang, X., Wang, T., Zhuang, B., and Xie, M.: Regional modeling of secondary organic aerosol over  
510 China using WRF/Chem, *Journal of Aerosol Science*, 43, 57-73, <http://dx.doi.org/10.1016/j.jaerosci.2011.09.003>,  
511 2012.

512 Kong, X., Forkel, R., Sokhi, R. S., Suppan, P., Baklanov, A., Gauss, M., Brunner, D., Barò, R., Balzarini, A., Chemel, C.,  
513 Curci, G., Jiménez-Guerrero, P., Hirtl, M., Honzak, L., Im, U., Pérez, J. L., Pirovano, G., San Jose, R., Schlünzen, K. H.,  
514 Tsegas, G., Tuccella, P., Werhahn, J., Žabkar, R., and Galmarini, S.: Analysis of meteorology–chemistry interactions  
515 during air pollution episodes using online coupled models within AQMEII phase-2, *Atmospheric Environment*,  
516 <http://dx.doi.org/10.1016/j.atmosenv.2014.09.020>, 2014.

517 Lin, Y.-L., Farley, R. D., and Orville, H. D.: Bulk parameterization of the snow field in a cloud model, *Journal of Climate*

518 and Applied Meteorology, 22, 1065-1092, 1983.

519 Liu, X.-H., Zhang, Y., Cheng, S.-H., Xing, J., Zhang, Q., Streets, D. G., Jang, C., Wang, W.-X., and Hao, J.-M.:  
520 Understanding of regional air pollution over China using CMAQ, part I performance evaluation and seasonal variation,  
521 Atmospheric Environment, 44, 2415-2426, 2010.

522 Makar, P. A., Gong, W., Milbrandt, J., Hogrefe, C., Zhang, Y., Curci, G., Žabkar, R., Im, U., Balzarini, A., Baró, R.,  
523 Bianconi, R., Cheung, P., Forkel, R., Gravel, S., Hirtl, M., Honzak, L., Hou, A., Jiménez - Guerrero, P., Langer, M.,  
524 Moran, M. D., Pabla, B., Pérez, J. L., Pirovano, G., San José R., Tuccella, P., Werhahn, J., Zhang, J., and Galmarini, S.:  
525 Feedbacks between Air Pollution and Weather, Part 1: Effects on Weather, Atmospheric Environment,  
526 <http://dx.doi.org/10.1016/j.atmosenv.2014.12.003>, 2014a.

527 Makar, P. A., Gong, W., Hogrefe, C., Zhang, Y., Curci, G., Žabkar, R., Milbrandt, J., Im, U., Balzarini, A., Baró, R.,  
528 Bianconi, R., Cheung, P., Forkel, R., Gravel, S., Hirtl, M., Honzak, L., Hou, A., Jiménez-Guerrero, P., Langer, M.,  
529 Moran, M. D., Pabla, B., Pérez, J. L., Pirovano, G., San José R., Tuccella, P., Werhahn, J., Zhang, J., and Galmarini, S.:  
530 Feedbacks between air pollution and weather, part 2: Effects on chemistry, Atmospheric Environment,  
531 <http://dx.doi.org/10.1016/j.atmosenv.2014.10.021>, 2014b.

532 Matsui, H., Koike, M., Kondo, Y., Takegawa, N., Kita, K., Miyazaki, Y., Hu, M., Chang, S. Y., Blake, D. R., Fast, J. D.,  
533 Zaveri, R. A., Streets, D. G., Zhang, Q., and Zhu, T.: Spatial and temporal variations of aerosols around Beijing in  
534 summer 2006: Model evaluation and source apportionment, J. Geophys. Res.-Atmos., 114, D00G13,  
535 10.1029/2008jd010906, 2009.

536 Mlawer, E. J., Taubman, S. J., Brown, P. D., Iacono, M. J., and Clough, S. A.: Radiative transfer for inhomogeneous  
537 atmospheres: RRTM, a validated correlated - k model for the longwave, Journal of Geophysical Research:  
538 Atmospheres (1984–2012), 102, 16663-16682, 1997.

539 Molders, N., Tran, H. N. Q., Cahill, C. F., Leelasakultum, K., and Tran, T. T.: Assessment of WRF/Chem PM2.5 forecasts  
540 using mobile and fixed location data from the Fairbanks, Alaska winter 2008/09 field campaign, Atmos. Pollut. Res., 3,  
541 180-191, 10.5094/apr.2012.018, 2012.

542 Morrison, H., Thompson, G., and Tatarki, V.: Impact of cloud microphysics on the development of trailing stratiform  
543 precipitation in a simulated squall line: Comparison of one-and two-moment schemes, Monthly Weather Review, 137,  
544 991–1007, doi: 10.1175/2008MWR2556.1, 2009.

545 Rosenfeld, D., Lohmann, U., Raga, G. B., O'Dowd, C. D., Kulmala, M., Fuzzi, S., Reissell, A., and Andreae, M. O.: Flood  
546 or drought: how do aerosols affect precipitation?, science, 321, 1309-1313, 2008.

547 Schell, B., Ackermann, I. J., Hass, H., Binkowski, F. S., and Ebel, A.: Modeling the formation of secondary organic aerosol  
548 within a comprehensive air quality model system, Journal of Geophysical Research: Atmospheres (1984–2012), 106,  
549 28275-28293, 2001.

550 Sun, Y., Jiang, Q., Wang, Z., Fu, P., Li, J., Yang, T., and Yin, Y.: Investigation of the sources and evolution processes of

551 severe haze pollution in Beijing in January 2013, *Journal of Geophysical Research: Atmospheres*, 119, 4380-4398,  
552 2014JD021641, 10.1002/2014JD021641, 2014.

553 Tao, W.-K., Chen, J.-P., Li, Z., Wang, C., and Zhang, C.: Impact of aerosols on convective clouds and precipitation, *Reviews*  
554 *of Geophysics*, 50, RG2001, 10.1029/2011RG000369, 2012.

555 Tuccella, P., Curci, G., Visconti, G., Bessagnet, B., Menut, L., and Park, R. J.: Modeling of gas and aerosol with WRF/Chem  
556 over Europe: Evaluation and sensitivity study, *J. Geophys. Res.-Atmos.*, 117, D03303, doi:10.1029/2011jd016302,  
557 2012.

558 Twomey, S.: The influence of pollution on the shortwave albedo of clouds, *Journal of the atmospheric sciences*, 34,  
559 1149-1152, 1977.

560 Wang, H., Zhang, X., Gong, S., and Xue, M.: The simulation study of the interaction between aerosols and heavy air  
561 pollution weather in East China, *AIP Conference Proceedings*, 1527, 499-502, doi:<http://dx.doi.org/10.1063/1.4803314>,  
562 2013.

563 Wang, L. T., Wei, Z., Yang, J., Zhang, Y., Zhang, F. F., Su, J., Meng, C. C., and Zhang, Q.: The 2013 severe haze over  
564 southern Hebei, China: model evaluation, source apportionment, and policy implications, *Atmos. Chem. Phys.*, 14,  
565 3151-3173, 10.5194/acp-14-3151-2014, 2014.

566 Wang, Y., and Zhou, L.: Observed trends in extreme precipitation events in China during 1961–2001 and the associated  
567 changes in large - scale circulation, *Geophysical Research Letters*, 32, L09707, doi:10.1029/2005GL022574, 2005.

568 Wang, Y. S., Yao, L., Wang, L., Liu, Z., Ji, D., Tang, G., Zhang, J., Sun, Y., Hu, B., and Xin, J.: Mechanism for the formation  
569 of the January 2013 heavy haze pollution episode over central and eastern China, *Science China Earth Sciences*, 1-12,  
570 2014.

571 Wang, Y. X., Zhang, Q., Jiang, J., Zhou, W., Wang, B., He, K., Duan, F., Zhang, Q., Philip, S., and Xie, Y.: Enhanced sulfate  
572 formation during China's severe winter haze episode in Jan 2013 missing from current models, *Journal of Geophysical*  
573 *Research: Atmospheres*, 119, 10425-10440, 10.1002/2013JD021426, 2014.

574 Wang, Z. F., Li, J., Wang, Z., Yang, W., Tang, X., Ge, B., Yan, P., Zhu, L., Chen, X., and Chen, H.: Modeling study of  
575 regional severe hazes over mid-eastern China in January 2013 and its implications on pollution prevention and control,  
576 *Science China Earth Sciences*, 57, 3-13, 2014.

577 Yahya, K., Wang, K., Gudoshava, M., Glotfelty, T., and Zhang, Y.: Application of WRF/Chem over North America under  
578 the AQMEII Phase 2: Part I. Comprehensive evaluation of 2006 simulation, *Atmospheric Environment*,  
579 doi:10.1016/j.atmosenv.2014.08.063, 2014.

580 Yang, Q., Gustafson Jr, W., Fast, J. D., Wang, H., Easter, R. C., Morrison, H., Lee, Y.-N., Chapman, E. G., Spak, S., and  
581 Mena-Carrasco, M.: Assessing regional scale predictions of aerosols, marine stratocumulus, and their interactions  
582 during VOCALS-REx using WRF-Chem, *Atmospheric Chemistry and Physics*, 11, 11951-11975, 2011.

583 Zaveri, R. A., and Peters, L. K.: A new lumped structure photochemical mechanism for large - scale applications, *Journal of*

584 Geophysical Research: Atmospheres (1984–2012), 104, 30387-30415, 1999.

585 Zaveri, R. A., Easter, R. C., Fast, J. D., and Peters, L. K.: Model for simulating aerosol interactions and chemistry  
586 (MOSAIC), *Journal of Geophysical Research: Atmospheres* (1984–2012), 113, D13204, doi:10.1029/2007JD008782,  
587 2008.

588 Zhang, J. K., Sun, Y., Liu, Z. R., Ji, D. S., Hu, B., Liu, Q., and Wang, Y. S.: Characterization of submicron aerosols during a  
589 month of serious pollution in Beijing, 2013, *Atmos. Chem. Phys.*, 14, 2887-2903, 10.5194/acp-14-2887-2014, 2014.

590 Zhang, Y., Zhang, X., Cai, C., Wang, K., and Wang, L.: Studying Aerosol-Cloud-Climate Interactions over East Asia Using  
591 WRF/Chem, in: *Air Pollution Modeling and its Application XXIII*, Springer, 61-66, 2014.

592 Zhang, Y., Bocquet, M., Mallet, V., Seigneur, C., and Baklanov, A.: Real-time air quality forecasting, part I: History,  
593 techniques, and current status, *Atmospheric Environment*, 60, 632-655, 10.1016/j.atmosenv.2012.06.031, 2012.

594 Zhang, Y., Wen, X.-Y., and Jang, C.: Simulating chemistry–aerosol–cloud–radiation–climate feedbacks over the continental  
595 US using the online-coupled Weather Research Forecasting Model with chemistry (WRF/Chem), *Atmospheric  
596 Environment*, 44, 3568-3582, 2010.

597 Zhao, C., Liu, X., Ruby Leung, L., and Hagos, S.: Radiative impact of mineral dust on monsoon precipitation variability  
598 over West Africa, *Atmospheric Chemistry and Physics*, 11, 1879-1893, 2011.

599 Zhao, C., Liu, X., and Leung, L.: Impact of the Desert dust on the summer monsoon system over Southwestern North  
600 America, *Atmospheric Chemistry and Physics*, 12, 3717-3731, 2012.

601 Zhou, G., Yang, F., Geng, F., Xu, J., Yang, X., and Tie, X.: Measuring and Modeling Aerosol: Relationship with Haze Events  
602 in Shanghai, China, *Aerosol and Air Quality Research*, 14, 783-792, 2014.

603

<b>CASE name</b>	<b>Characteristics</b>
BASE	With all aerosol feedbacks
RAD	Only with aerosol direct and semi-direct effects
EMP	Without any aerosol feedbacks

**Table 2.** Statistical Performance of baseline simulations for meteorology.

	<b>T2 (°C)</b>	<b>RH2 (%)</b>	<b>WS10 (m/s)</b>	<b>PM2.5 (µg/m<sup>3</sup>)</b>
N of stations	523	523	523	71
Mean OBS	-1.8	66	1.9	129.2
Mean SIM	-2.8	66	3.9	111.5
Corr. R	0.96	0.47	0.47	0.67
MB	-1.0	0	2.0	-18.9
NMB	-0.4% <sup>*</sup>	<0.1%	105%	-15.0%
RMSE	3.4	16	2.7	30.7

608      \* Calculated in K.

609

610 **Table 3.** Observed and simulated enhancement ratios of PM<sub>2.5</sub>. The enhancement ratio is defined as the average of daily  
611 PM<sub>2.5</sub> larger than the median value divided by that of hourly PM<sub>2.5</sub> less than the median value during the month. NCP, YRD,  
612 PRD, and CC represent the North China Plain, the Yangtze River Delta, the Pearl River Delta, and Central China,  
613 respectively.

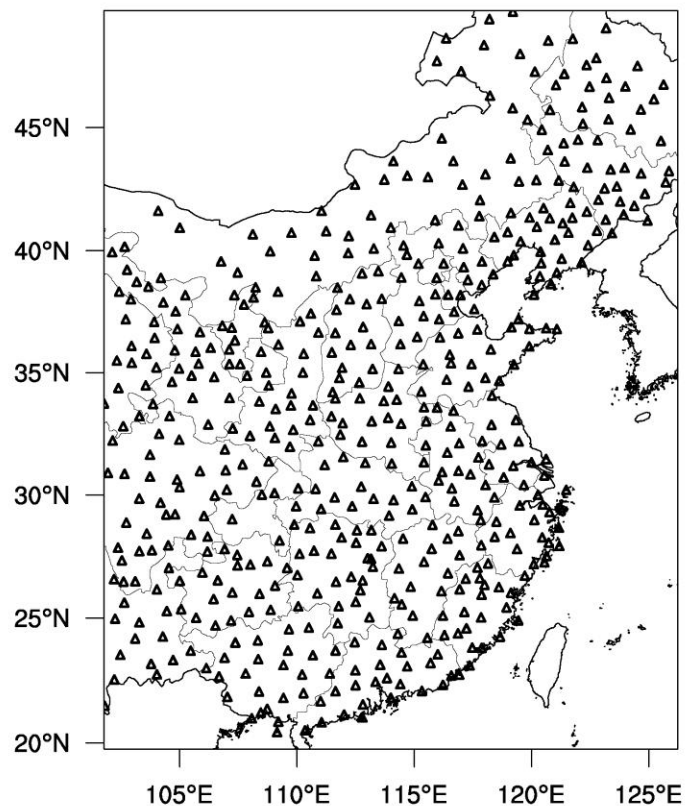
	NCP	YRD	PRD	CC
Observations	1.7	1.6	1.5	1.7
WRF-Chem (BASE)	1.6	1.7	1.6	1.7

614  
615

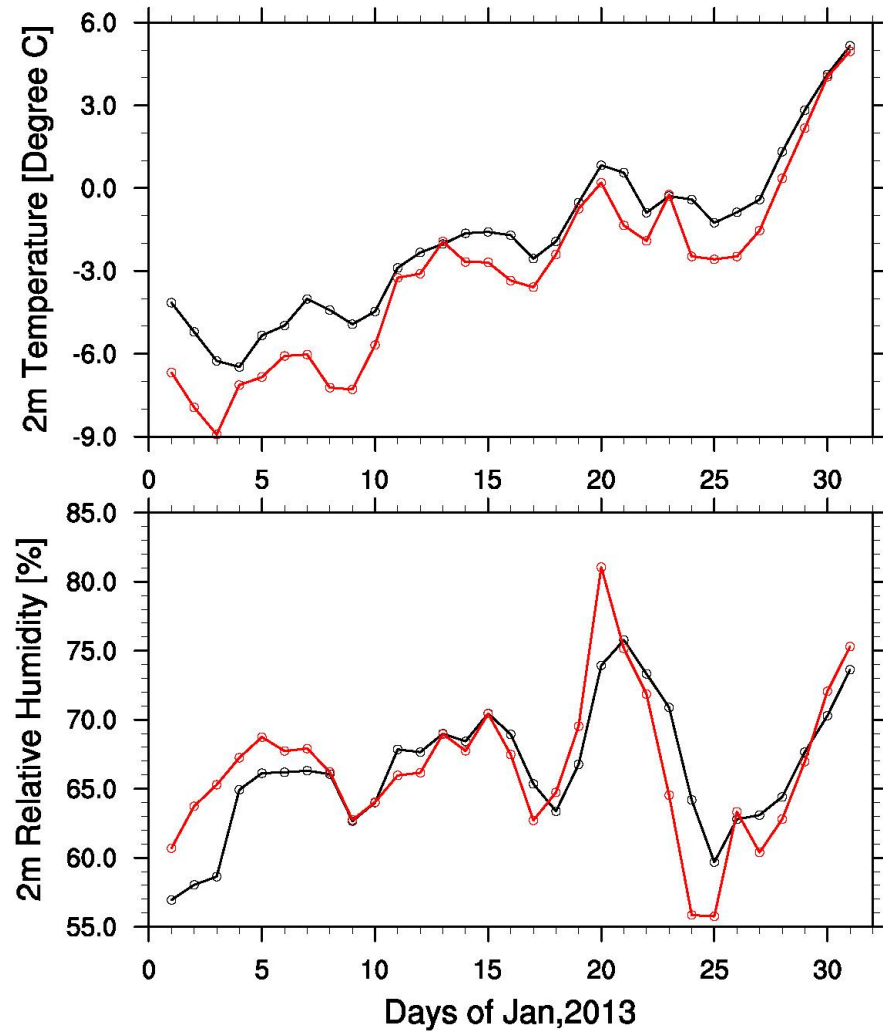
616 **Table 4.** Modeled SOA, OA and PM<sub>2.5</sub> using MADE/SORGAM and MOSAIC in comparison with observations. The data  
617 shown are spatially averaged over 71 big cities and temporally averaged during January 6~10, 2013.

	SOA (μg/m <sup>3</sup> )	OA (μg/m <sup>3</sup> )	SOA/OA	PM <sub>2.5</sub> (μg/m <sup>3</sup> )	NMB of PM <sub>2.5</sub>
MADE/SORGAM	0.3	9.4	2.8%	68.3	49.7%
MOSAIC				115.4	15.0%
Observations				135.7	

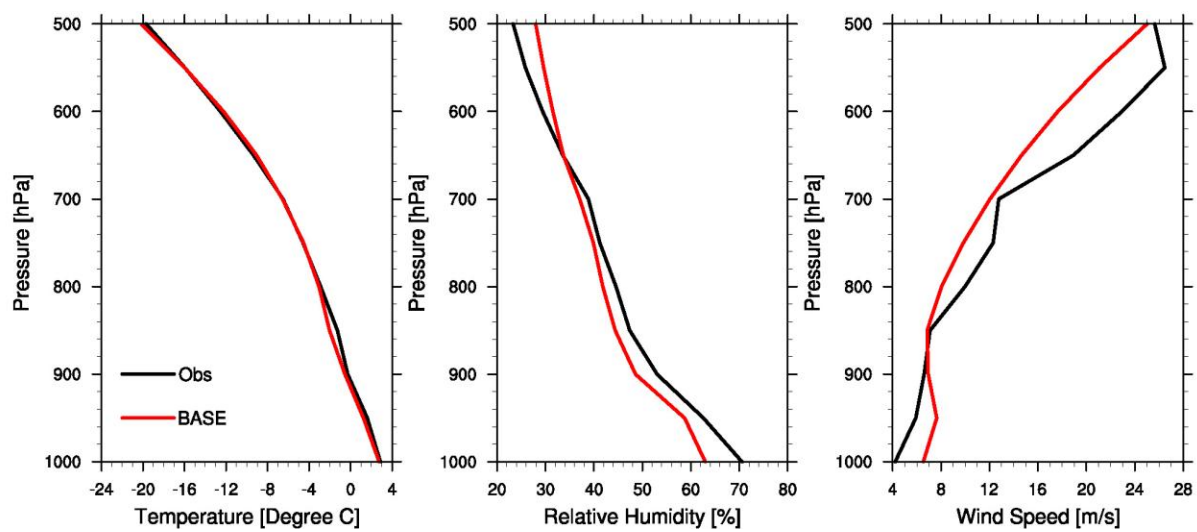
618  
619



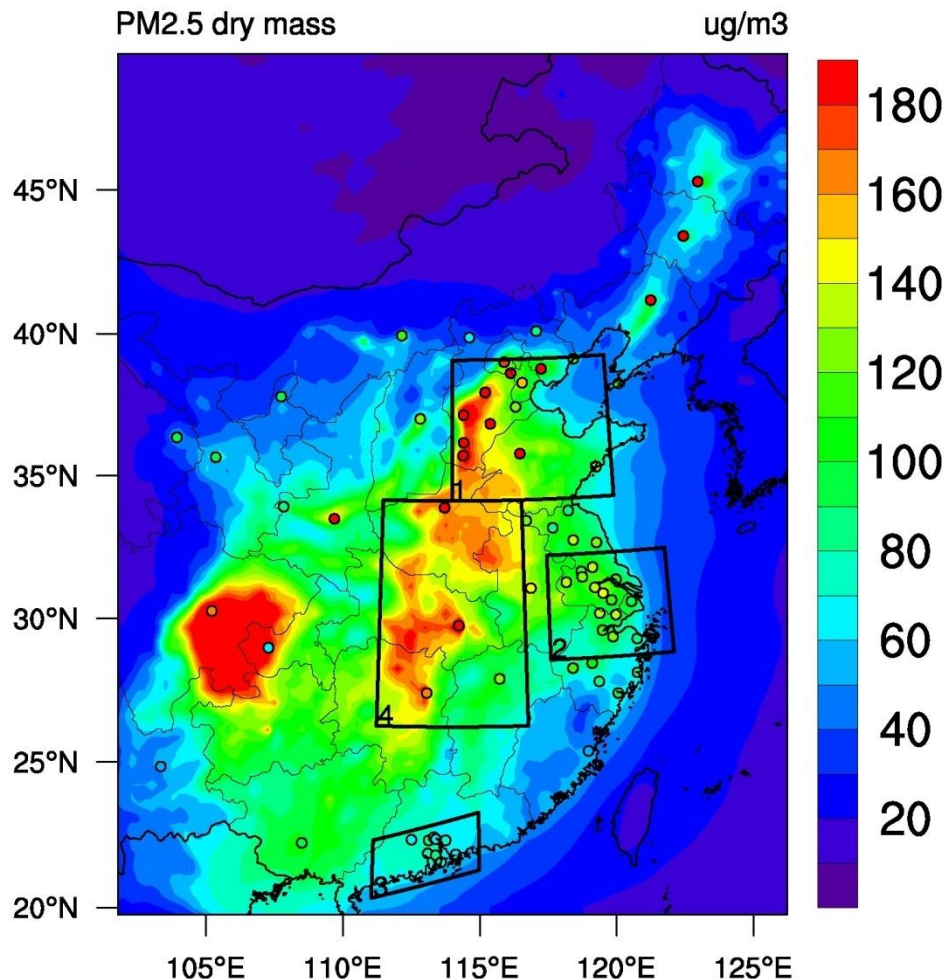
620  
621 **Fig 1.** WRF/Chem modeling domain with grid resolution of 27 km. The domain covers eastern parts of China. The triangles  
622 indicates the location of 523 meteorology stations used for evaluations in this work.  
623



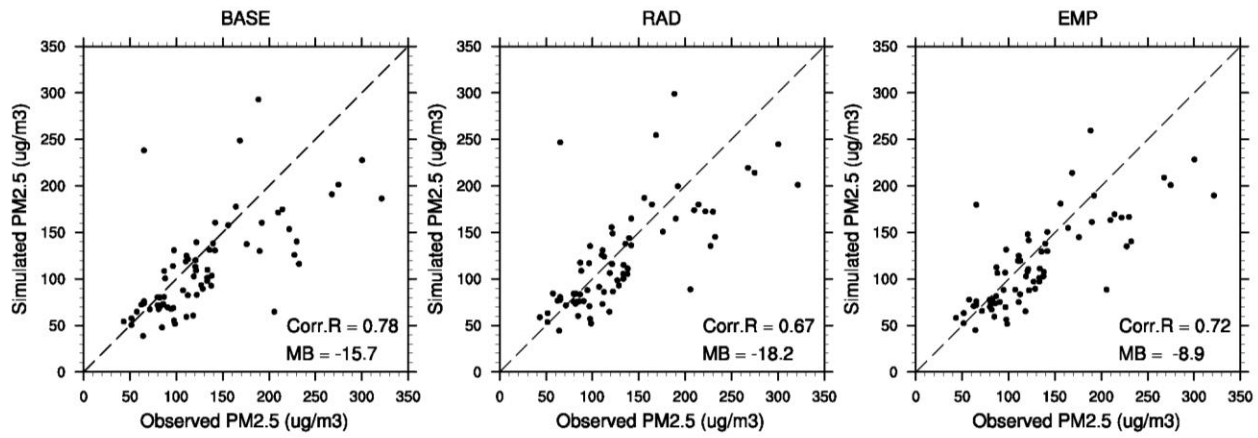
624  
625 **Fig 2.** Time series of observed (black line) and simulated (red line) daily meteorological variables averaged over 523  
626 meteorology stations in January 2013.  
627  
628



631 **Fig 3.** Monthly mean vertical profiles of observed (black line) and simulated (red line) meteorological variables averaged  
 632 over 36 meteorology stations.



636 **Fig 4.** Simulated and Observed (circles) monthly mean PM<sub>2.5</sub> mass concentration over eastern China in January 2013. The  
 637 four polygons stands for the North China Plain (NCP) (#1), the Yangtze River Delta (YRD) (#2), the Pearl River Delta  
 638 (PRD) (#3), and Central China (#4).



640  
641 **Fig 5.** Scatter plots of monthly mean PM<sub>2.5</sub> mass concentrations in 71 cities in January 2013.  
642

## Temporal Variations of PM<sub>2.5</sub>

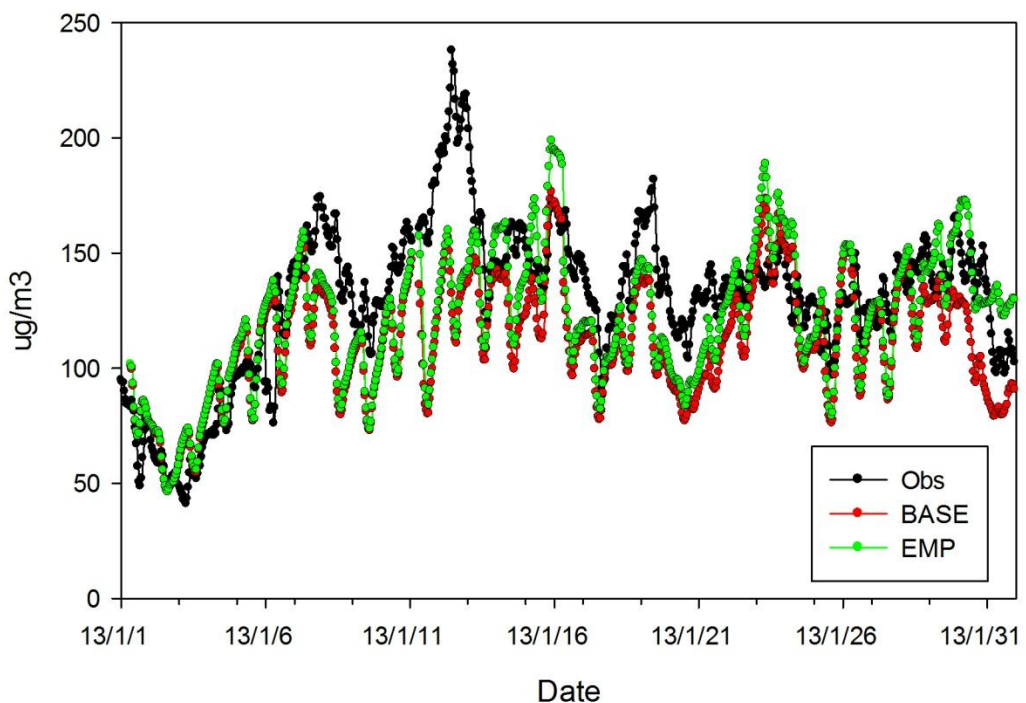
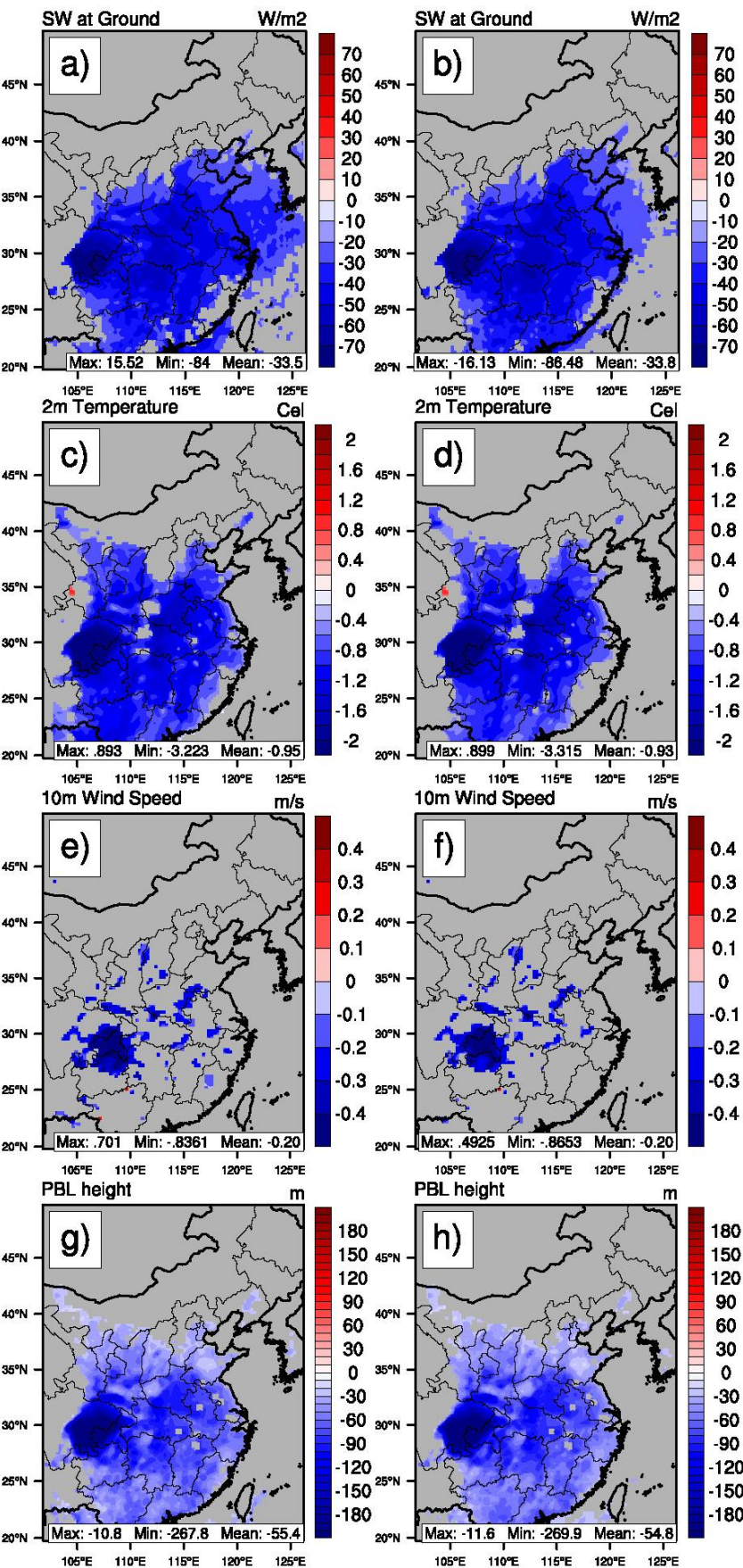
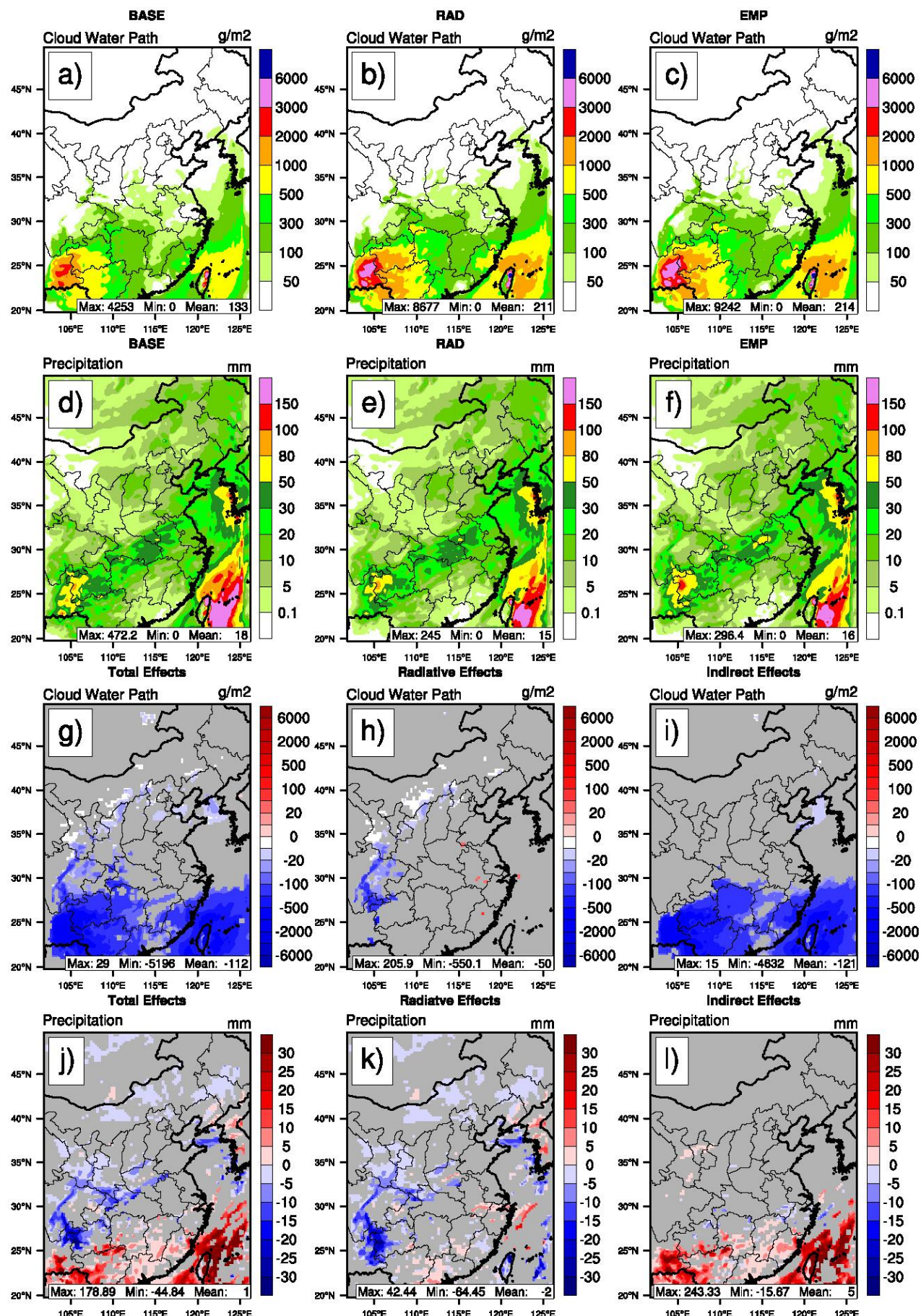


**Fig 6.** Comparison of observed (black) and simulated (red for the BASE scenario and blue for the EMP scenario) hourly near surface PM<sub>2.5</sub> mass concentrations averaged over 71 cities in China in January 2013.

## Total Effects      Radiative Effects



648  
 649 **Fig 7.** Simulated aerosol total effects (BASE - EMP) and radiative effects (RAD - EMP) on downward short wave flux at  
 650 ground, 2m temperature, 10 m wind speed and PBL height in January 2013. The aerosol indirect effects on these four  
 651 meteorological variables are not shown here, since the induced changes are not significant according to Student's t-test.  
 652 Grey shaded areas indicate regions with less than 95% significance.



655 **Fig 8.** Simulated cloud water path (a-c) and precipitation (d-f) for the three scenarios and aerosol total effects (BASE –  
656 EMP) (g and j), radiative effects (RAD – EMP) (h and k), and indirect effects (BASE – RAD) (i and l) over eastern China  
657 in January 2013. Grey shaded areas indicate regions with less than 95% significance.

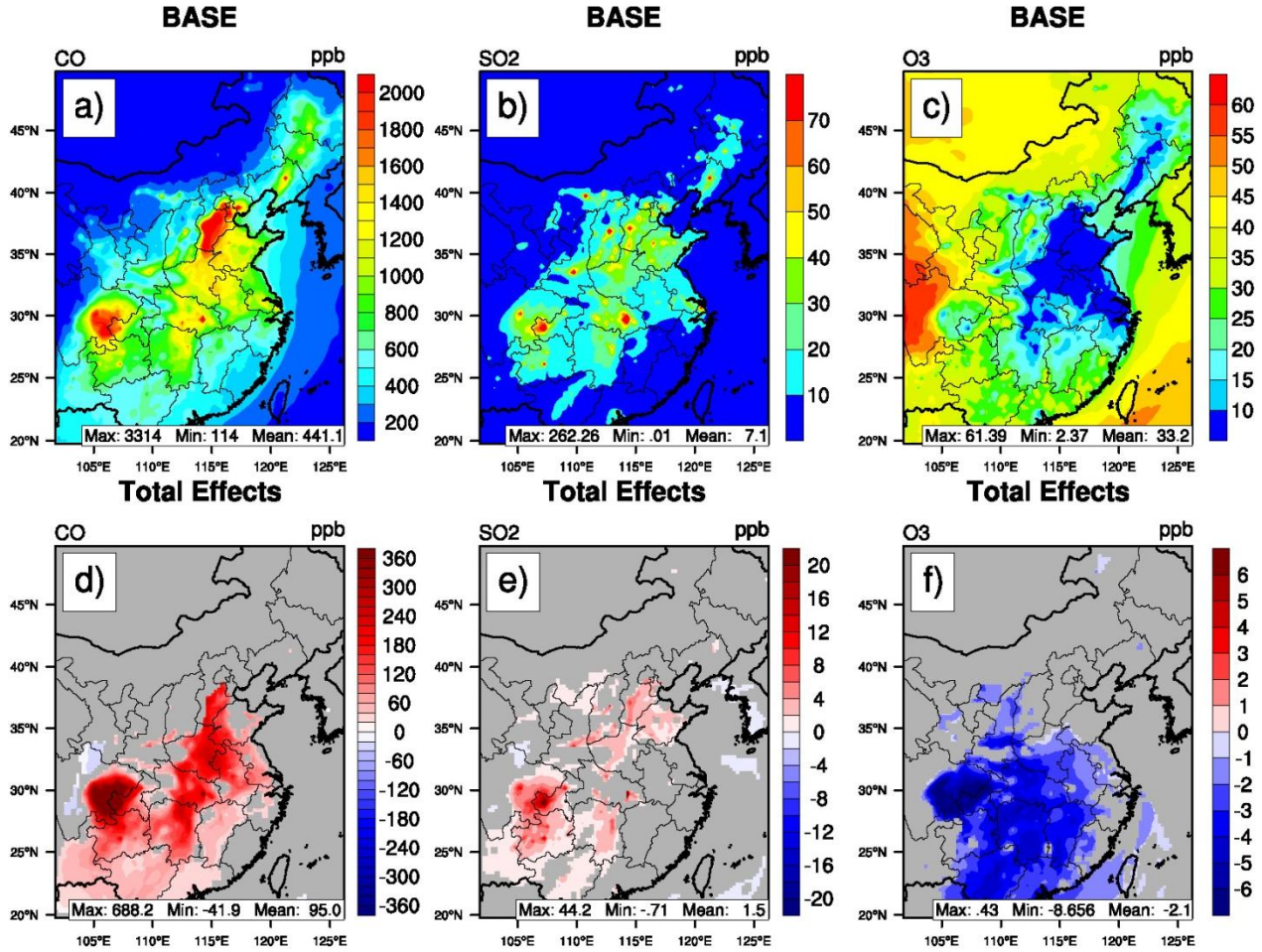


Fig. 9. Simulated monthly mean CO, SO<sub>2</sub>, and O<sub>3</sub> mixing ratios and aerosol feedbacks (BASE - EMP) on the three gas pollutants over eastern China in January 2013. Grey shaded areas indicate regions with less than 95% significance.

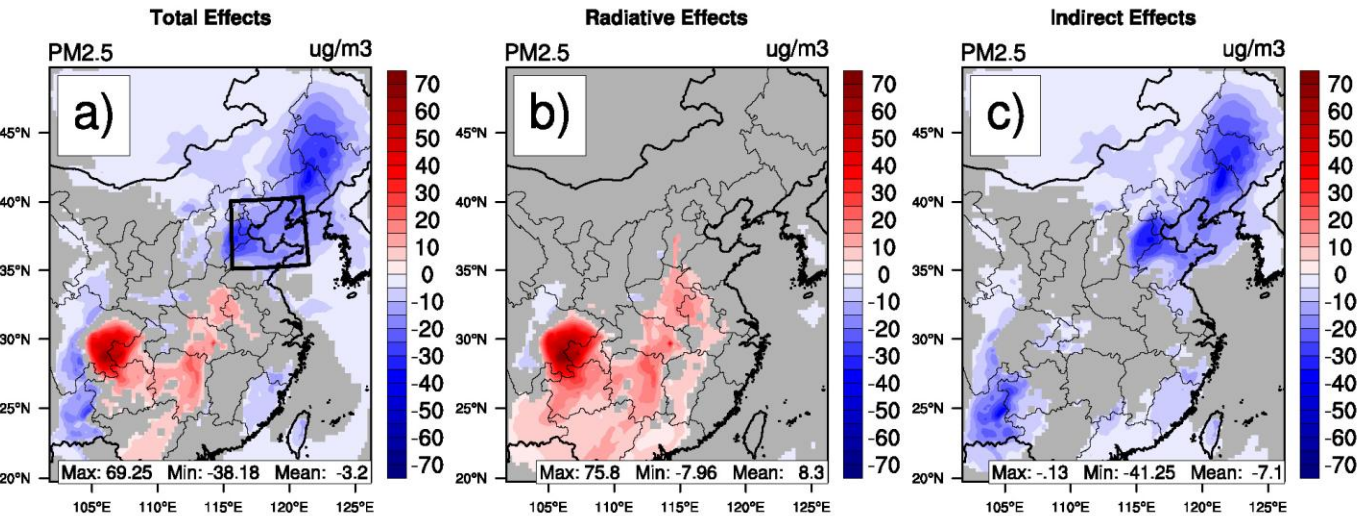
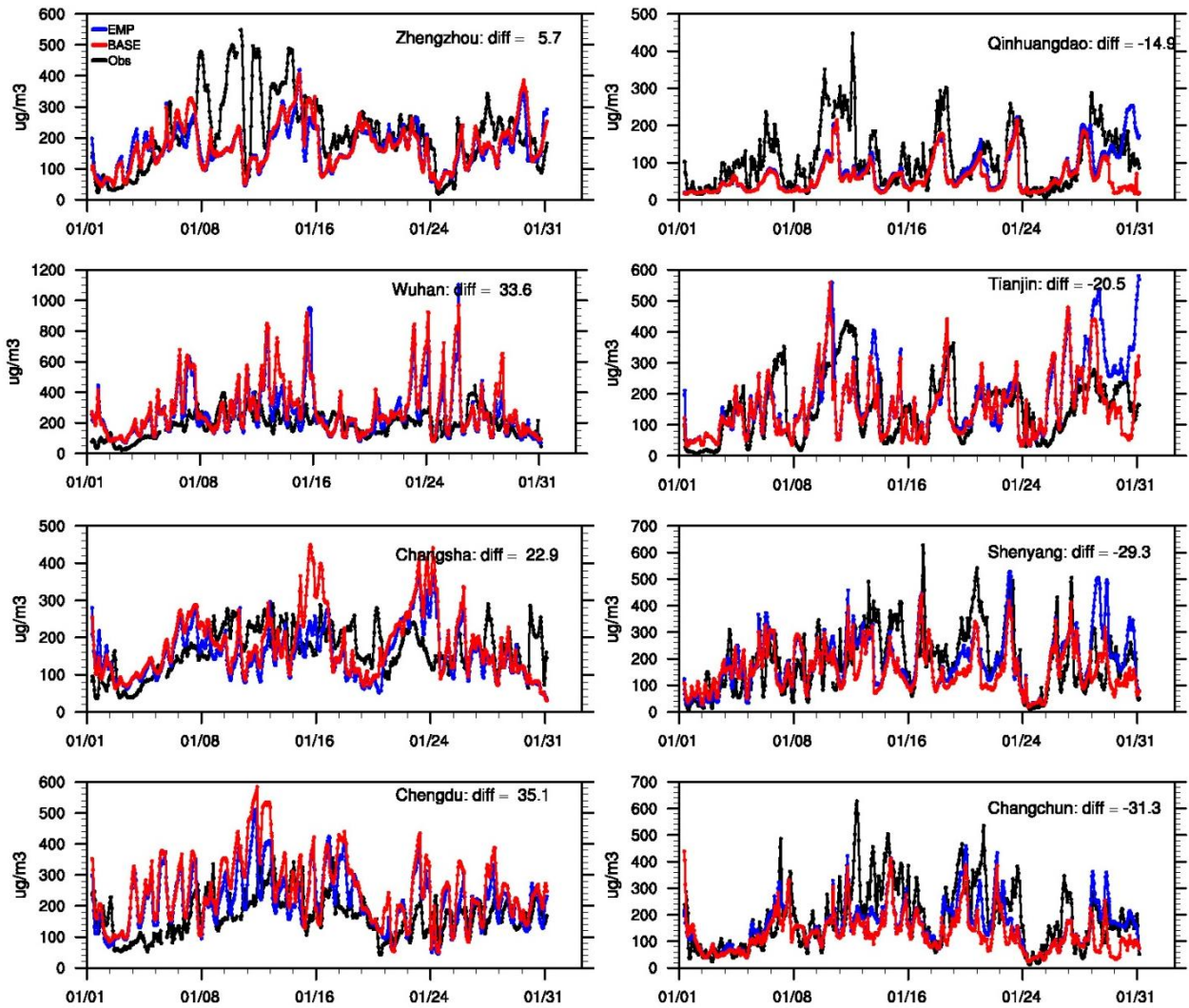
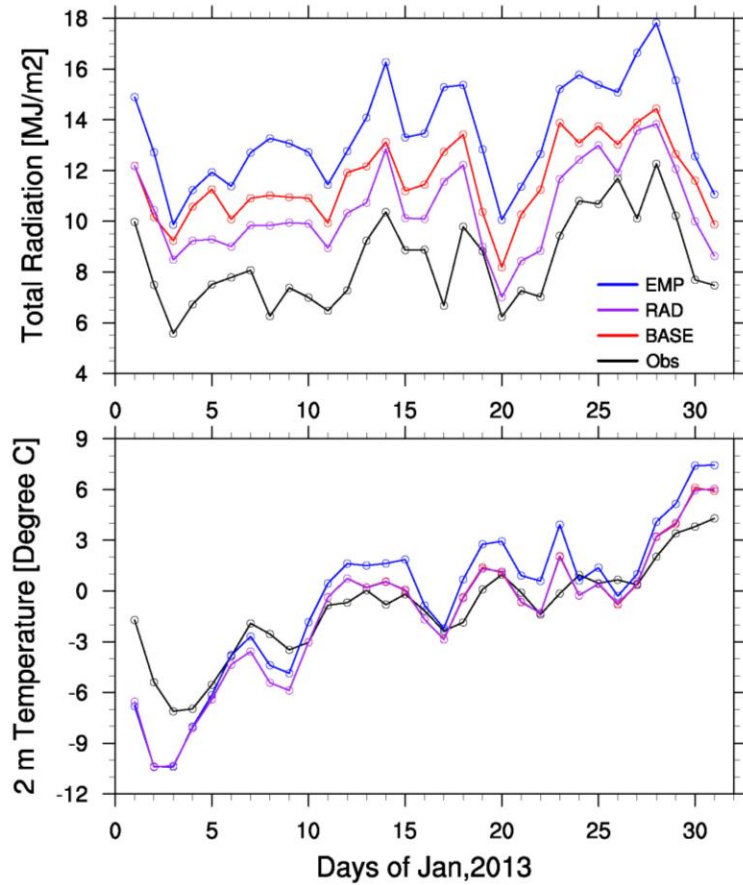


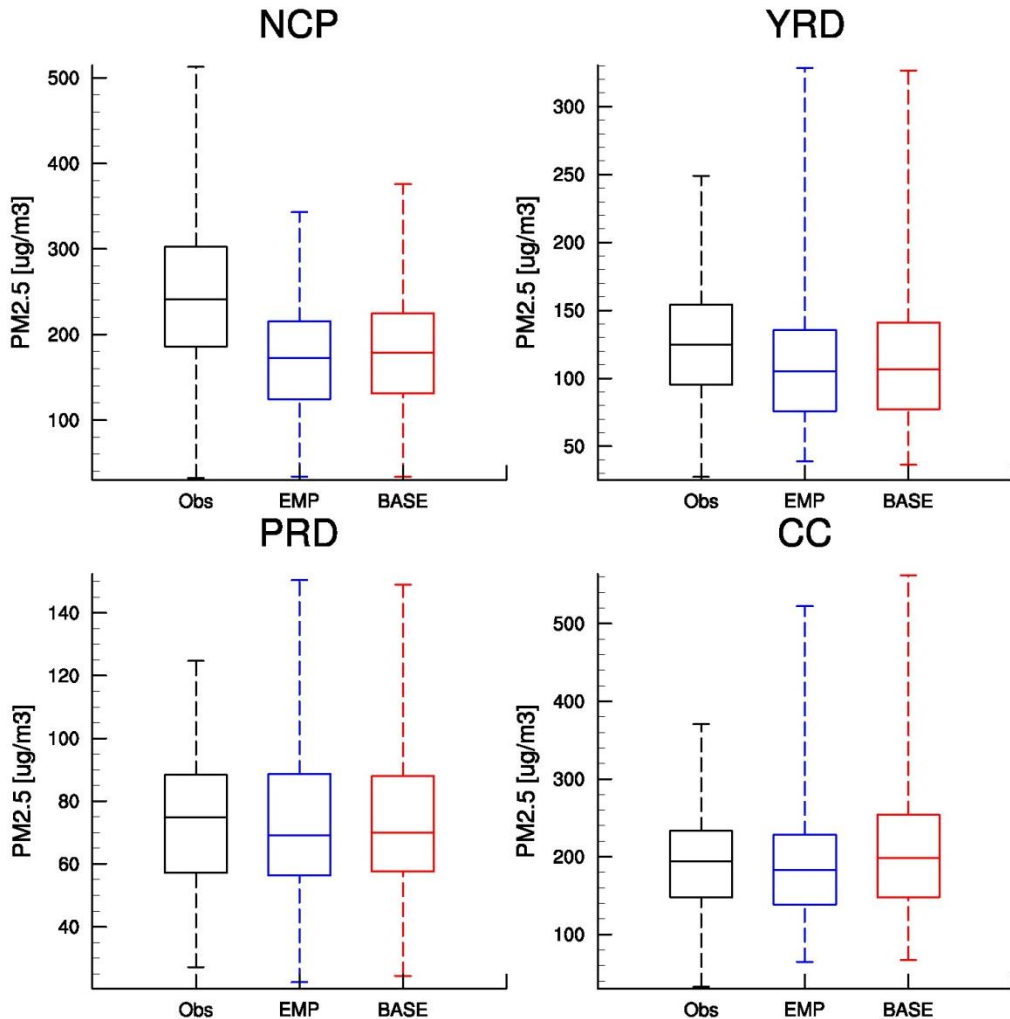
Fig 10. Simulated aerosol total effects (BASE – EMP), radiative effects (RAD – EMP), and indirect effects (BASE – RAD) on monthly mean  $\text{PM}_{2.5}$  over eastern China in January 2013. Grey shaded areas indicate regions with less than 95% significance. The black polygon defines the Bohai Sea surrounding area.



670  
671 **Fig 11.** Time series of observed (black) and simulated (red for BASE scenario and blue for EMP scenario) hourly surface  
672 PM<sub>2.5</sub> mass concentrations in 8 cities in January 2013. Monthly mean PM<sub>2.5</sub> are enhanced in the four cities (Zhengzhou,  
673 Wuhan, Changsha and Chengdu) in the left column. Cities in the right column have suppressed monthly mean PM<sub>2.5</sub> mass  
674 concentrations. “Diff” indicates aerosol feedbacks (BASE – EMP) on monthly mean PM<sub>2.5</sub> mass concentrations.  
675



676  
677 **Fig 12.** Time series of observed (black) and simulated (red for the BASE scenario, purple for the RAD scenario, and blue  
678 for the EMP scenario) daily total radiation and 2 m temperature averaged over North and central China in January 2013.  
679



681 **Fig 13.** Observed (black) and Simulated (red for the BASE scenario and blue for the EMP scenario) monthly mean PM<sub>2.5</sub>  
682 mass concentrations in January 2013 over the North China Plain (NCP), the Yangtze River Delta (YRD),  
683 the Pearl River Delta (PRD) and Central China (CC). The dashed lines indicate the maximum and minimum value.  
684 The solid lines in the box indicate the median value (the central line), the 25<sup>th</sup> and 75<sup>th</sup> percentiles.